Magnetic excitations in Ho_2Co_{17} and Ho_2Fe_{17}. An inelastic neutron scattering study

Clausen, Kurt Nørgaard

Publication date:
1981

Document Version
Publisher's PDF, also known as Version of record

RISØ

Risø-R-426

Magnetic Excitations in Ho_2Co_{17} and Ho_2Fe_{17}

An Inelastic Neutron Scattering Study

K. N. Clausen

Risø National Laboratory, DK-4000 Roskilde Denmark
January 1981

RISØ-R-426

MAGNETIC EXCITCATIONS IN Ho_2Co_{17} AND Ho_2Fe_{17} AN INELASTIC NEUTRON SCATTERING STUDY

K.N. Clausen

Abstract. The low energy part (<20 meV) of the magnetic excitation spectrum of the uniaxial easy basal plane ferrimagnets Ho_2Co_{17} and Ho_2Fe_{17} have been measured along the three high symmetry directions at a temperature of 4.2 K, using the inelastic neutron scattering technique. The resulting magnon dispersion relations have been interpreted using linear spin wave theory with a Hamiltonian including single ion crystal field anisotropy and isotropic exchange between spatially well localized spins, i.e. we have used a localized pseudo spin description of the magnetism of the itinerant 3d-ions. The R_2T_{17} structure contains two different Ho sites, with the same point symmetry, and from the spin wave results it was concluded that the crystal field anisotropy of the two Ho sites in both Ho_2Co_{17} and Ho_2Fe_{17} were identical. The deduced crystal field parameters for Ho_2Fe_{17} were slightly larger than for Ho_2Co_{17}, and the parameters were of the same order of magnitude as for pure Ho. For Ho_2Fe_{17} the Fe-Fe exchange was found to be anisotropic, and for both compounds the magnetic ordering temperatures T_C of 1178 K for Ho_2Co_{17} and 335 K for Ho_2Fe_{17} were determined by the strong positive 3d-3d exchange. The rare earth - 3d exchange constant, which is respon-

(continue on next page)

January 1981

Risø National Laboratory, DK 4000 Roskilde, Denmark

sible for the ferrimagnetic coupling scheme was observed to be small and negative, and within experimental uncertainty identical for the two compounds. The rare earth - rare earth exchange in both cases found to be negligible, and consequently, a non dispersive crystal field like excitation was observed. Using the parameters deduced from the linear spin-wave fit to the observed magnon dispersive relations, the temperature dependence of the non dispersive modes and the magnetization curve (the latter only for Ho_2Co_{17} because data was not available for Ho_2Fe_{17}) could be predicted and was found to agree with experiments. The low temperature (4.2 K) macroscopic anisotropy constants predicted from the deduced crystal field parameters were an order of magnitude larger than the experimentally observed values.

UDC 546.665 : 537.226.4 : 539.171.4.017

This report is submitted to the Technical University of Denmark in partial fulfilment of the requirements for obtaining the lic.techn. (Ph.D.) degree.

ISBN 87-550-0658-2
ISSN 0106-2840

Risø Repro 1981

CONTENTS

page

INTRODUCTION

Using the inelastic neutron scattering technique, the low energy part (< 20 meV) of the magnon dispersion relations in the uniaxial easy basal plane ferrimagnets Ho_2Co_{17} and Ho_2Fe_{17} have been investigated at a temperature of 4.2 K. Only three branches of very simple shape were observed: a highly dispersive mode of parabolic shape, a non-dispersive mode, and a dispersive mode degenerate with the q-independent mode at the zone-boundary. From the observed three branches, only six microscopic parameters describing the magnetic interactions can be deduced. We have described both the rare earth and the transition metal spins in a localised picture and using a linear spin-wave model with a Hamiltonian including isotropic exchange and single ion crystal field anisotropy we have deduced the following six parameters from a general least squares fit to the observed data: J_{TT}, J_{RT}, J_{TT} (the nearest neighbour transition metal-transition metal, rare earth-transition metal and rare earth-rare earth exchange constants), $B_2^0(R)$, $B_6^6(R)$ (the crystal field parameters for the rare earth sites), and $B_2(T)$ (a parameter describing the anisotropy of the transition metal sublattice).

The 3d-3d exchange constant J_{TT} was found to be dominant in the two-ion interactions, and within the experimental uncertainty the observed ordering temperatures T_c of 1178 K (Ho_2Co_{17}) and 335 K (Ho_2Fe_{17}) could be predicted from J_{TT} using the mean field approximation. For Ho_2Fe_{17} the 3d-3d exchange was found to be anisotropic, and different values of J_{TT} had to be used for the three different high-symmetry directions, in order to explain the observed data.

Within the experimental uncertainty the deduced rare earth transition metal exchange constants J_{RT} were identical for the two compounds. J_{RT} is the only parameter coupling the two sublattices together, and the magnetization curve is therefore sensitive to the actual magnitude of J_{RT}. For Ho_2Co_{17} (data not available for Ho_2Fe_{17}) the observed magnetization curve could be reproduced from the deduced parameters within the experimental accuracy.

The rare earth-rare earth exchange constant was found to be negligible in both Ho_2Co_{17} and Ho_2Fe_{17}.

From the actual number of observed modes (three instead of five) it was concluded that the crystal field parameters for the two Ho sites were identical. This indicated that the anisotropy of the Ho sites are dominated by the influence of the group of nearest neighbour transition metal atoms, which is identical for the two sites, rather than by the more distant Ho surroundings, which differs for the two sites. The anisotropy constants $B_2^0(R)$, $B_6^6(R)$ are slightly larger for Ho_2Fe_{17} than for Ho_2Co_{17}, but in both cases values typical for rare earth metals were found. From $B_2^0(R)$, $B_6^6(R)$, and the rare earth transition metal exchange constant J_{RT}, the observed temperature-dependent scattering from the non-dispersive excitations could be predicted.

The description of the transition metal anisotropy by a localised model is very rough, but qualitatively the results show that the anisotropy of the transition metal sublattice favoured an easy basal plane, and that the contribution from the 3d-metal could not be neglected, especially for Ho_2Co_{17}. For Ho_2Fe_{17} the appearance of the two-ion anisotropy complicates the picture and makes conclusive statements of the single ion Fe anisotropy impossible.

The macroscopic anisotropy parameters predicted from the microscopic crystal field parameters were overestimated by an order of magnitude.

In the First Chapter of this thesis the microscopic model and the general magnetic properties of the rare earth transition metal compounds are reviewed. In Chapter Two a general linear spin-wave model for a uniaxial ferrimagnet is derived, and in Chapter Three the experimental set-up is presented and the observed magnon dispersion relation interpreted in terms of the linear spin-wave model. In Chapter Four the observed temperature dependence of the localised modes, the macroscopic anisotropy constants, and the magnetisation curve (the latter only for Ho_2Co_{17}) are compared with the corresponding properties pre-

dicted on the basis of the parameters deduced from the linear spin wave fit. In Chapter Five the adequacy of the model and the final conclusions are discussed. In Appendices A to C the detailed deduction of the spin wave model is presented.

1. RARE EARTH - 3d COMPOUNDS - MICROSCOPIC MODEL

In this chapter we first define the group of compounds which are denoted the rare earth - transition metals or the rare earth - 3d intermetallics, and secondly, we discuss the microscopic Hamiltonian which will be used to interpret our experimental data. In the last part of the chapter a discussion of the magnetic interactions and a review of the observed ordering temperature, ordered magnetic moments, and structures of the rare earth Fe and Co compounds are given.

1.1. The rare earth - 3d compounds

The rare earth - 3d intermetallics are a group of compounds with well defined stoichiometries and crystal structures. The general formula is R_nT_m where R denotes Y or any of the lanthanides, while T represents a 3d element, Mn, Fe, Co or Ni. From four to eight different compositions (n, m) have been observed in the range from the pure rare earth metals to the pure transition metals.

For all these R_nT_m compounds, ternary, and quarternary compounds - with the same crystal structures - can be found by partial substitution of the rare earth or the transition metal or both, with other rare earth and 3d ions, and consequently the rare earth - 3d intermetallics cover a very large family of compounds. In this study we will limit ourselves to those R_nFe_m and R_nCo_m compounds which exhibit the highest ordering temperatures.

1.2. The microscopic Hamiltonian

We have examined the ground-state spin-wave dispersion relations and the temperature dependence of the localised, crystal field excitations in Ho_2Co_{17} and Ho_2Fe_{17}. The experimental results will be interpreted using linear spin-wave theory and mean field theory, both based on an empirical Hamiltonian H, including isotropic exchange H_{EX} and single ion crystal field anisotropy H_{CF}.

$$H = H_{EX} + H_{CF}$$

$$= - \sum_{ij} J_{ij} \underline{J}_i \cdot \underline{J}_j + \sum_i \sum_{\ell,m} B_\ell^m(i) \; O_\ell^m(i) \qquad (1)$$

The exchange constants J_{ij} and the coefficients $B_\ell^m(i)$ of the symmetry-determined Stevens operator expansion (Hutchings, 1964) of H_{CF} is to be determined from the experiments. In this model the magnetic interactions are assumed to operate between spatially well-localised spins $\underline{J}_i$.

For the rare earth ions, $\underline{J}$ is the total angular momentum of the tripositive ion, determined by Hunds rules, and $B_\ell^m(i)$ is the crystal field parameter of ion number i. The Hamiltonian (1) is known to be a very good first approximation for pure rare earth systems, and for compounds containing both non-magnetic ions and rare earth ions. The correction terms to the Hamiltonian H - the two ion anisotropy and the magnetostriction - are assumed to be small, and to have only negligible influence on the excitation spectra for Ho_2Fe_{17} and Ho_2Co_{17}.

The magnetism of the itinerant transition metal ions cannot generally be explained by a localised model, but when only ground-state magnetic excitations are considered, the localised model has been successfully applied by Rhyne and Koon (1978) to the cubic $HoFe_2$ compound. Furthermore a band theoretical discussion of spin waves in itinerant ferro and antiferromagnets by Liu (1976) showed that in the ground state there is a spin density cloud around each ion site. When a spin-wave is excited this spin cloud precesses as a rigid unit, which was denoted a quasi-spin.

Consequently, we feel quite confident in using a localised model for the interpretation of ground state spin-waves in Ho_2Co_{17} and Ho_2Fe_{17}.

For the transition metal ions we have defined the quasi-spin $\underline{J}$ through the relation

$$\underline{\mu} = -g\ \mu_B\ \underline{J} \qquad (2)$$

where $\underline{\mu}$ is the observed magnetic moment, μ_B is the Bohr magneton and the g factor was defined as 2.00. In the pseudo spin picture defined via (2), $B_\ell^m(i)$ for the i'th transition metal ion can be considered only as an expansion parameter, i.e. it should not be quoted as a crystal field parameter.

1.3. The magnetic moments of the 3d-ions

The observed magnetic moments of the transition metal ions in the Y_xT_{1-x} and Gd_xT_{1-x} compounds are shown in Fig. 1. For all Co compounds with $x < 0.20$ the magnetic moment μ_{Co} is very close to 1.7 μ_B per atom, which is the ordered moment for pure Co (Betteridge, 1979). For $x > 0.20$, μ_{Co} depends heavily on both the stoichiometry and the rare earth ion in the compound. When x is larger than 0.3 the ordered moment of Co is zero unless the rare earth partner is magnetic, i.e. in this case the presence of a magnetic moment on the rare earth ion can induce a spin polarization of the transition metal 3d band. In the Fe compounds the dependence of μ_{Fe} on both stoichiometry and the rare earth ion in the compounds is much less pronounced, and as the rare earth content x is increased, a slow decrease in μ_{Fe} from 2.2 μ_B per atom is observed. The ordered moment for pure Fe is 2.2 μ_B per atom (Betteridge, 1979).

The magnetic moments of the rare earth-3d intermetallics should be discussed in terms of band theory. However, because of the complicated crystal structures, and the approximations which have to be introduced, in order to include the interactions with the localised 4f electrons (for which the band description is in-

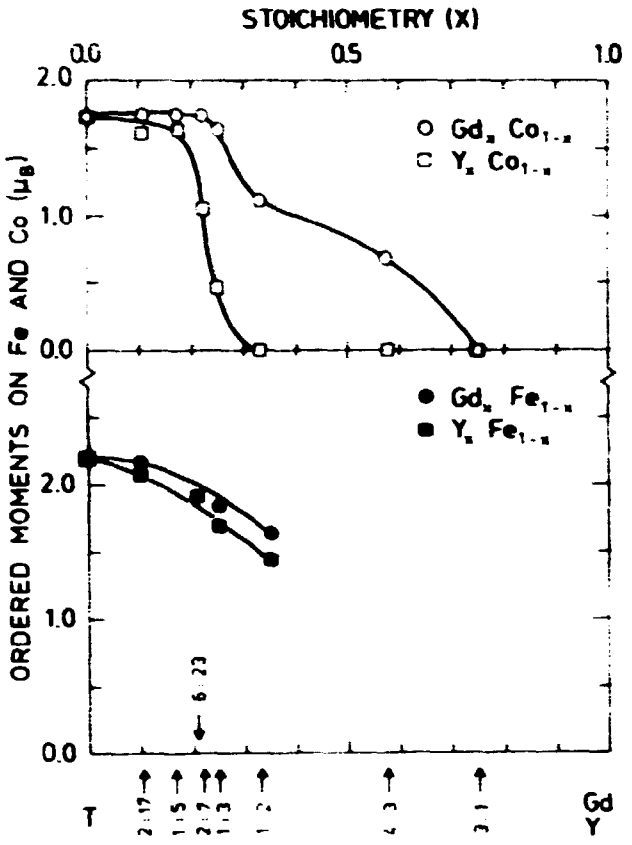

Fig. 1. Ordered magnetic moments on the 3d metal in R_nT_m compounds as a function of x = n/(n+m). The actual n:m values of the compounds are shown underneath the figure. R is either non-magnetic Y or magnetic Gd. The data was obtained from magnetisation measurements (Kirchmayer and Poldy, 1978). The solid lines are guides for the eye.

applicable), only very few spin-polarized energy band structure calculations have been published. For YCo_5, $SmCo_5$, and $GdCo_5$ Malik (1977) found 3d bands almost identical to those in pure Co, and in an experimental study of the ternary compounds $Y_2(Fe,Co)_{17}$ and $Y_2(Co,Ni)_{17}$, Taylor and Poldy (1975) found an average 3d magnetic moment (Fig. 2) in good agreement with the Slater-Pauling curve (solid line in Fig. 2) (Bozorth, 1951), which has been derived for the pure 3d metals using a rigid band model. On the basis of these results, it is generally believed that for the transition metal rich Fe and Co compounds (all Fe compounds and Co compounds for $x < 0.2$), the 3d bands are almost identical to the pure Fe and Co 3d bands.

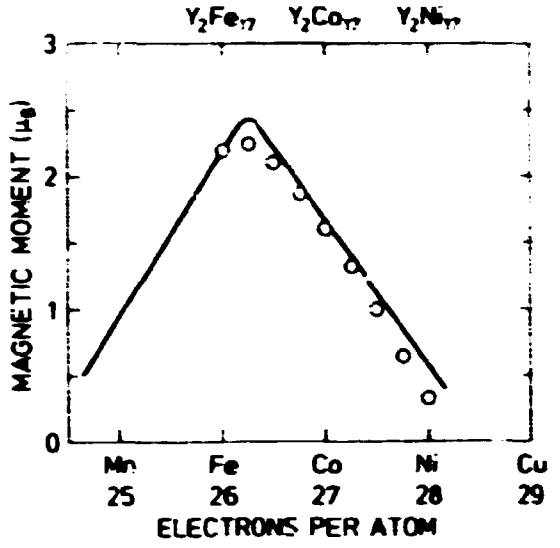

Fig. 2. The average magnetic moment in $Y_2(Fe,Co)_{17}$ and $Y_2(Co,Ni)_{17}$ ternaries as a function of electron concentration. The solid line is the Slater-Pauling curve, (Bozorth, 1951) and the data points are from Taylor and Poldy (1975).

1.4. Exchange interactions in the R_nT_m compounds

The origin of the exchange interaction is electrostatic, and it is introduced when the Coulomb repulsion between the two electrons in the hydrogen molecule is considered. The requirement that the wave functions should be antisymmetric leads to a splitting of the ground state into a triplet and a singlet state. This splitting can be calculated using the Heisenberg Hamiltonian

$$H = - J_{12} \underline{S}_1 \cdot \underline{S}_2$$

where

$$J_{12} = (E_S - E_T)$$

E_S and E_T are the energies of the singlet and the triplet state, and $\underline{S}_1$ and $\underline{S}_2$ are the spins of the two electrons. For a general magnetic system the Heisenberg Hamiltonian represents the lowest-order expansion of the two-ion interactions in terms of the total ionic angular momentum. In this case the exchange constant is merely an expansion coefficient, the sign and magnitude of which should be determined from experiments.

Since the spatial extension of the transition metal 3d wave functions are much larger than the extension of the well localised rare earth 4f wave functions, three different exchange mechanisms have to be considered in the rare earth transition metal compounds. The transition metal - transition metal exchange is a direct interaction caused by the overlap of nearest neighbour 3d wave functions, whereas the rare earth - transition metal and the rare earth - rare earth exchange both are indirectly mediated via other electrons in the system. A more detailed discussion of the three exchange mechanisms is given in Sections 1.4.1. to 1.4.3.

The appearance of magnetic long range order in the R_nT_m compounds is an effect of the two ion interactions, and the ordering temperature is a measure of the magnitude of the exchange interactions. Figure 3 shows the ordering temperatures T_C for all Fe

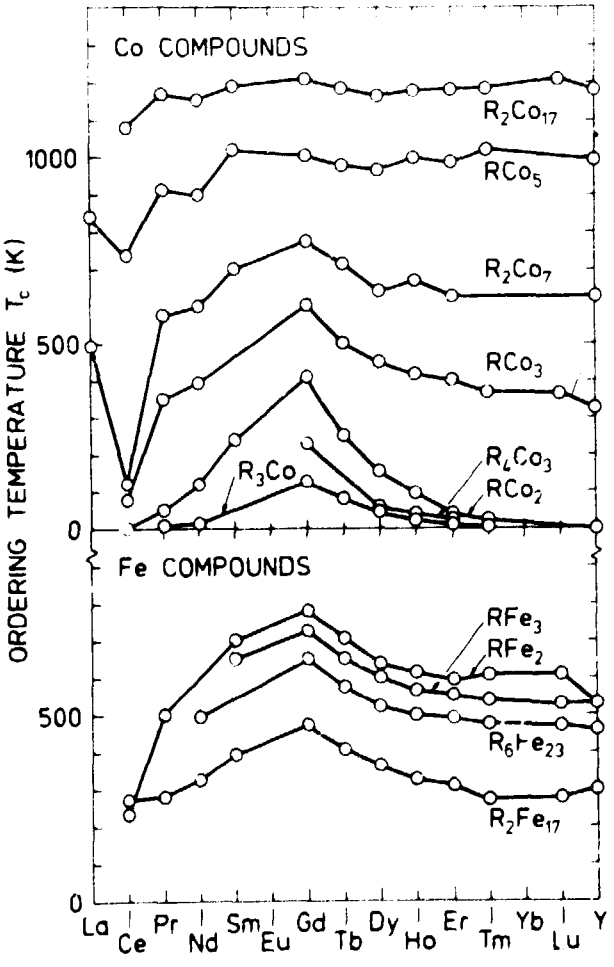

Fig. 3. Magnetic ordering temperatures T_c for R_nFe_m and R_nCo_m compounds as a function of the rare earth ion. The data are from review articles by Wallace (1973) and Kirchmayer and Poldy (1978). The solid lines are guides for the eye.

and Co compounds. In Fig. 4, T_C is shown as a function of stoichiometry for Y_xT_{1-x} and Gd_xT_{1-x}. In the discussion of the ordering temperatures we will neglect the Ce compounds, because the valency of the Ce ions might differ from 3. The ordering temperatures of the Co compounds R_xCo_{1-x} with $x \lesssim 0.25$ is determined mainly by the stoichiometry, and is almost independent of the rare earth ions, i.e. the 3d-3d exchange interactions are dominant. For $x > 0.25$ the rare earth plays an important role, and for all the Fe compounds the dominant exchange interaction is operating between the Fe ions.

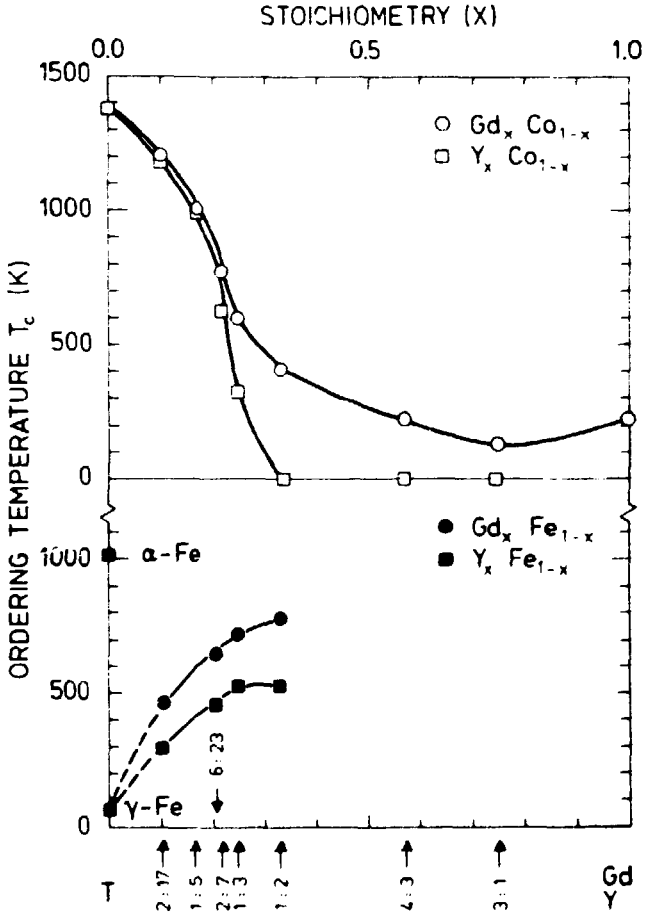

Fig. 4. The ordering temperatures of R_xCo_{1-x} and R_xFe_{1-x} as a function of stoichiometry. The data are from Wallace (1973) and Kirchmayer and Poldy (1978). The solid line is a guide for the eye. In the rare earth rich R_xCo_{1-x} ($x > 0.20$) compounds the presence of a magnetic moment on the rare earth ion can induce a magnetic moment on the transition metal.

1.4.1. The transition metal - transition metal exchange

For the transition metal-rich R_nT_m compounds the 3d-3d exchange is dominant and, as for pure Fe and Co, J_{TT} is positive, leading to a ferromagnetic coupling of the transition metal sublattice. The exchange constant J_{TT} can be estimated from the ordering temperatures T_C and the pseudo-spin J_T using the nearest neighbour mean field approximation

$$J_{TT}^{MF} = \frac{3\ k_B\ T_C}{N \cdot J_T(J_T+1)} \qquad (3)$$

where k_B is Boltzmann's constant and N is the number of interacting 3d ions (the number of nearest transition metal neighbours).

For the pure transition metals Bethe (1933) and Slater (1930) have used the Heitler-London description of the 3d wave functions to give a qualitative description of the 3d-3d exchange interaction as a function of the normalised interatomic distance R/R_o where R_o is the radius of the 3d shell. Several other authors have presented an empirical constructed quantitative Bethe-Slater curve (solid line in Fig. 5) derived from experimental data on the effects of compression, structural changes, and alloying of the 3d metals (see e.g. Animalu, 1977). In Fig. 5 we have also plotted the calculated (using Eq.(3) and Table 1) mean field exchange constant J_{TT}^{MF} for the transition metal rich Y_xCo_{1-x} and Y_xFe_{1-x} as a function of the minimum transition metal separation R_{3d-3d}^{min} normalized with the radius R_o of the 3d shell for pure Co and Fe respectively, i.e. we have here used the assumption that the 3d bands of Fe and Co were only slightly changed on alloying with Y. The only purpose of Fig. 5 and the arguments above is to give a very sketchy justification for using the Bethe-Slater curve to qualitatively explain the dependence of the ordering temperature on the stoichiometry (Fig. 4).

For Co, RCo_5, and R_2Co_{17} J_{Co-Co} is constant and the decrease in T_C on increasing rare earth content is a consequence of the decrease in the number of nearest Co neighbours. For the Fe compounds two competing effects occur: The dilution with rare earth tends to decrease T_C, but the decrease in the minimum Fe-Fe sep-

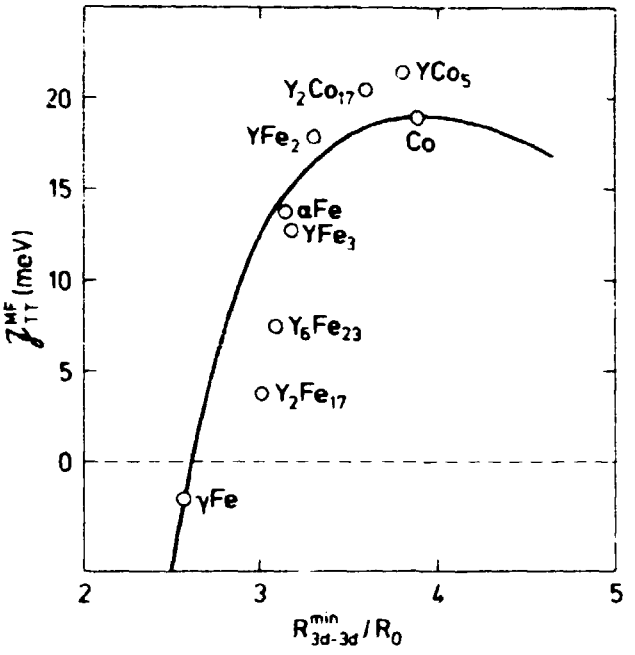

Fig. 5. The average nearest neighbour mean field exchange constant as a function of the normalised minimum 3d-3d distance. The solid line is the Bethe-Slater curve taken from Animalu (1977). The data on Y_nT_m compounds in which only T-T exchange is present, are taken from Table 1.

aration on increasing Fe content causes a large decrease in J_{Fe-Fe}. As the latter effect is the strongest, T_C is increased on decreasing the Fe content (see Fig. 4).

1.4.2. The rare earth - transition metal exchange

Two different mechanisms have been proposed for the rare earth -3d exchange. Buschow (1971) has suggested a long-range indirect RKKY-type mechanism mediated via the conduction electrons, i.e. involving s-f and s-d interactions. From band calculations on $GdCo_5$ and $SmCo_5$, Malik (1977) on the other hand found a short-range interaction between the 3d electrons and the nearest neighbour 4f electrons via the 4d or 5d electrons of the rare earth ion (d-d coupling).

In both cases the exchange results in a negative spin-spin coupling, which can explain the observed uniaxial alignment of the

Table 1. For the transition metal rich Y_xT_{1-x} compounds we have tabulated the minimum transition metal separation d_{min}, the ordering temperature T_c, and the pseudo-spin $J_T = \mu_T/2\cdot\mu_B$. Several of these compounds contain more than one transition metal site, and N is the average number of nearest neighbours. J_{TT}^{MF} is the mean field nearest neighbour exchange constant calculated from Eq.(3) and d_{min}/R_o^T is the normalised transition metal separation. The normalisation constant R_o^T is the radius of the 3d shell (R_o^{Fe} = 0.79Å and R_o^{Co} = 0.65Å). α-Fe is the naturally occurring ferromagnetic bcc-Fe. γ-Fe is the antiferromagnetic fcc-Fe observed only under high pressure. The data are taken from Wallace (1973), Animalu (1977), and Gubbens (1977).

Compound	d_{min} (Å)	T_c (K)	J_T	N	J_{TT}^{MF} (meV)	d_{min}/R_o^T
Co	2.51	1394	0.86	12	18.9	3.88
Y_2Co_{17}	2.32	1180	0.80	10.4	20.5	3.59
YCo_5	2.45	1000	0.80	8.4	21.4	3.79
γFe		∿70	∿0.50	12	-2.0	2.57
Y_2Fe_{17}	2.37	335	1.05	10.4	3.8	3.00
Y_6Fe_{23}	2.44	460	0.95	8.7	7.4	3.09
αFe	2.48	1043	1.11	8.0	13.7	3.14
YFe_3	2.50	520	0.85	6.7	12.8	3.17
YFe_2	2.60	520	0.73	6	17.9	3.29

magnetic moments in the transition metal rich R_nT_m compounds. The transition metal sublattice is ferromagnetically aligned because of the 3d-3d exchange and the spins of the rare earth ions are coupled antiparallel to the 3d spins, leading to ferromagnetic structures for compounds with the light lanthanides and ferrimagnetic structures for compounds with the heavy rare earth elements.

1.4.3. The rare earth - rare earth exchange

The rare earth - rare earth exchange is identical to the long range oscillatory RKKY interaction (Ruderman and Kittel, 1954) observed in the pure rare earth systems. In the indirect RKKY exchange interactions the presence of a spin on the rare earth

ions creates a net oscillatory spin density in the itinerant conduction electron gas. This causes an indirect exchange between the rare earth ions, and when the transition metal sublattice is non magnetic (e.g. R_4Co_3, see Kirchmayr and Poldy, 1978), both the exchange and the crystal field interactions are as in the pure rare earth metals (i.e. both the ordering temperatures and the observed non-collinear antiferromagnetic structures are typical for rare earth compounds with a non magnetic element). If, on the other hand, the transition metal sublattice is magnetic, then the itinerant electron bands are spin polarised and the 4f-4f exchange negligible. This agrees with the experimental fact that in all transition metal rich R_nT_m compounds, it is a very good approximation to neglect the rare earth - rare earth exchange.

1.5. The crystal field anisotropy

The charges of the surrounding ions in a crystal produce an electric field, the so-called crystalline electric field, at any ion. The presence of this field causes a preferential orientation of the magnetic moments along certain crystallographic directions, because the direction of the magnetic moment is coupled to the non-spherically symmetric wave functions of the magnetic ions via spin-orbit coupling. In other words, the crystal field interaction is a result of the Coulomb repulsion between the surrounding ions and the charge distribution of the magnetic ion. The effect of this interaction is to produce a single-ion magnetic anisotropy. In the transition metal rich R_nT_m compounds the uniaxial alignment of the magnetic moments were determined by the exchange interactions, but the actual crystallographic direction of the easy axis is determined by the crystal field anisotropy.

1.5.1. The crystal field anisotropy for the rare earth sites

The crystal field Hamiltonian for the rare earth sites can be expanded in Stevens operators O_ℓ^m, where the number of non zero crystal field parameters B_ℓ^m in the expansion is determined by the point symmetry of the actual site (Hutchings, 1964). In the hexagonal R_nT_m compounds, the point symmetry of the rare earth ion

is hexagonal, and the c-axis representation of the crystal field Hamiltonian contains four expansion coefficients (Wallace et al., 1977)

$$H_{CF}\ (R) = B_2^0\ O_2^0 + B_4^0\ O_4^0 + B_6^0\ O_6^0 + B_6^6\ O_6^6 \qquad (4)$$

The B_2^0 term is usually dominant, and this term has been estimated using a point charge model considering only the effect of rare earth nearest neighbours. (Creedan and Rao, 1973). Point charge calculations are, however, extremely uncertain for metallic systems, and the results should be regarded only as an indication of the sign of B_2^0.

For very low temperatures, the anisotropy of the rare earth transition metal compounds are generally dominated by the rare earth contribution to the crystal field anisotropy, but for room temperature and above the 3d sublattice contribution often dominates the anisotropy.

1.5.2. The crystal field anisotropy for the 3d sites

In the hexagonal R_nT_m compounds, the point symmetry of the transition metal sites is almost hexagonal, and since the spin of the 3d ions is small it is a good approximation to neglect the higher order terms (see Eq. 4), i.e.

$$H_{CF}\ (T) = B_2^0\ O_2^0\ ,$$

Whereas the rare earth contribution to the magnetic anisotropy is of the same order of magnitude as in pure rare earth metals, the Co contribution to the anistropy can be much larger (e.g. RCo_5) than in pure Co. Szpunar and Lindgård (1979) found the origin of this large contribution to be a result of the large change in the c/a ratio (compared to the close packed value $\sqrt{8/3}$) for the hexagonal (hcp) symmetry of the Co ions, which occurs when rare earth ions are present.

In the pseudo spin picture we will use a $B_2^0\ O_2^0$-like expansion of crystal field interactions in terms of the pseudo spin $\underline{J}_T$.

$$H_{CF}\ (T) = B_2(T)\ \left[3\ (J_T^z)^2 - J_T\ (J_T + 1)\right] \qquad (5)$$

2. LINEAR SPIN WAVE THEORY FOR A UNIAXIAL FERRIMAGNET

In this chapter the theory of linear spin-waves in a uniaxial antiferromagnet (Kittel, 1963) is extended to the case of a uniaxial ferrimagnet. In the first section the notation is defined and in the preceding sections we sketch the transformation of the Hamiltonian given in Eq. (1) expressed in terms of spin variables to a Hamiltonian in spin-wave variables, and the subsequent solution of the linear spin-wave problem. The details of the calculations are given in Appendices A to C.

2.1. Notation

The Hamiltonian describing the magnetic interactions - isotropic exchange and single ion crystal field anisotropy - was given in Eq. (1). With the quantisation along the z-axis, and the usual spin raising and lowering operators $J_j^+ = J_j^x + iJ_j^y$ and $J_j^- = J_j^x - iJ_j^y$ the Hamiltonian can be rewritten as:

$$\begin{aligned} \mathcal{H} &= -\sum_{ij} J_{ij}\ \underline{J}_i \cdot \underline{J}_j + \sum_i H_{CF}^i \\ &= -\sum_{ij} J_{ij}\left(\frac{1}{2}\left(J_i^+ J_j^- + J_i^- J_j^+\right) + J_i^z J_j^z\right) + \sum_i \sum_{\ell,m} B_\ell^m(i)\ O_\ell^m(i) \end{aligned} \qquad (6)$$

In the preceding chapter we saw that the two-ion interactions between two transition metal ions, a transition metal ion and a rare earth ion, and between two rare earth ions, were totally different, and that the single ion crystal field anisotropy was

determined by the ion and the point symmetry of the actual site. We will therefore introduce a notation which in an easy way allows us to distinguish between a rare earth and a transition metal ion, and between different sites of the rare earth and transition metal sublattices. Each single ion quantity will be identified by three parameters, and the two-ion exchange constant by six, according to the following scheme:

$$\underline{r}_\alpha^i(\underline{\ell}) = \underline{\ell} + \underline{d}_\alpha^i$$

$$J_i^+ = J_\alpha^{i+}(\underline{\ell})$$

$$J_i^- = J_\alpha^{i-}(\underline{\ell})$$

$$J_i^z = J_\alpha^{iz}(\underline{\ell})$$

$$J_{ij} = J_{\alpha\beta}^{ij}(\underline{\ell},\underline{m})$$

where

$\underline{\ell},\underline{m}$	are lattice vectors
α,β	denotes either rare earth (R) or transition metal (T)
i,j	is used to enumerate the position of a given type of atom within its unit cell
$\underline{r}_\alpha^i(\underline{\ell})$	is the position of the i'th atom of type α in the unit cell defined by the lattice vector $\underline{\ell}$
$\underline{d}_\alpha^i$	is the position of the i'th atom of type α within the unit cell.

2.2. Transformation of the Hamiltonian into magnon variables

In a ferrimagnetic compound, the Holstein-Primakoff transformation (Holstein and Primakoff, 1940) of the two sublattices differs (see Appendix A) because the quantisation axes of the two subsystems are antiparallel. If we denote the Bose creation and annihilation operators for the rare earth sublattice as $a_i(\underline{\ell})$,

$a_i^\dagger(\underline{\ell})$, and for the transition metal sublattice $b_j(\underline{m})$, $b_j^\dagger(\underline{m})$, the Holstein-Primakoff transformation can be written as (Appendix A)

$$J_R^{i+}(\underline{\ell}) = \sqrt{2J_R}\, a_i^\dagger(\underline{\ell}) \sqrt{1 - a_i^\dagger(\underline{\ell})a_i(\underline{\ell})/2J_R}$$

$$J_R^{i-}(\underline{\ell}) = \sqrt{2J_R} \sqrt{1 - a_i^\dagger(\underline{\ell})a_i(\underline{\ell})/2J_R}\, a_i(\underline{\ell})$$

$$J_R^{iz}(\underline{\ell}) = -J_R + a_i^\dagger(\underline{\ell})a_i(\underline{\ell})$$

$$J_T^{j+}(\underline{m}) = \sqrt{2J_T} \sqrt{1 - b_j^\dagger(\underline{m})b_j(\underline{m})/2J_T}\, b_j(\underline{m})$$

$$J_T^{j-}(\underline{m}) = \sqrt{2J_T}\, b_j^\dagger(\underline{m}) \sqrt{1 - b_j^\dagger(\underline{m})b_j(\underline{m})/2J_T}$$

$$J_T^{jz}(\underline{m}) = J_T - b_j^\dagger(\underline{m})b_j(\underline{m})$$

In a neutron scattering experiment, the observed quantities are not directly related to the Bose operators themselves, but to the spin-wave variables - or magnon variables - $a_{\underline{q}}^i$, $a_{\underline{q}}^{i\dagger}$, $b_{\underline{q}}^j$, $b_{\underline{q}}^{j\dagger}$, which is the Fourier transforms of the Bose operators. We introduce the spin-wave variables through the relations (Appendix B)

$$a_i^\dagger(\underline{\ell}) = 1/\sqrt{N} \sum_{\underline{q}} \exp(-i\underline{q}\cdot\underline{r}_R^i(\underline{\ell}))\, a_{\underline{q}}^{i\dagger}$$

$$a_i(\underline{\ell}) = 1/\sqrt{N} \cdot \sum_{\underline{q}} \exp(i\underline{q}\cdot\underline{r}_R^i(\underline{\ell}))\, a_{\underline{q}}^i$$

$$b_j^\dagger(\underline{m}) = 1/\sqrt{N} \sum_{\underline{q}} \exp(i\underline{q}\cdot\underline{r}_T^j(\underline{m}))\, b_{\underline{q}}^{j\dagger}$$

$$b_j(\underline{m}) = 1/\sqrt{N} \sum_{\underline{q}} \exp(-i\underline{q}\,\underline{r}_T^j(\underline{m}))\, b_{\underline{q}}^j$$

where N is the number of unit cells in the system.

In Appendix B these transformations have been treated in detail, and the second-order expansion of the Hamiltonian in terms of magnon variables has been derived, (in linear spin-wave theory only second-order terms are taken into account), and the result is:

$$
\begin{aligned}
H = \sum_{\underline{q}} \Bigg[\sum_{ij} \Big\{ & J_T \Big(J^{ij}_{TT}(\underline{0}) [b^{i\dagger}_{\underline{q}} b^{i}_{\underline{q}} + b^{j\dagger}_{\underline{q}} b^{j}_{\underline{q}}] - 2\, J^{ij}_{TT}(\underline{q}) b^{i}_{\underline{q}} b^{j\dagger}_{\underline{q}} \Big) \\
& + J_R \Big(J^{ij}_{RR}(\underline{0}) [a^{i\dagger}_{\underline{q}} a^{i}_{\underline{q}} + a^{j\dagger}_{\underline{q}} a^{j}_{\underline{q}}] - 2\, J^{ij}_{RR}(\underline{q}) a^{i\dagger}_{\underline{q}} a^{j}_{\underline{q}} \Big) \\
& - 2\, J^{ij}_{RT}(\underline{0}) [J_R\, b^{j\dagger}_{\underline{q}} b^{j}_{\underline{q}} + J_T\, a^{i\dagger}_{\underline{q}} a^{i}_{\underline{q}}] \\
& - 2 \sqrt{J_R J_T} \left(J^{ij}_{RT}(\underline{q}) a^{i\dagger}_{\underline{q}} b^{j\dagger}_{\underline{q}} + J^{ij}_{RT}(-\underline{q}) a^{i}_{\underline{q}} b^{j}_{\underline{q}} \right) \Big\} \\
& + \sum_{i} \Big\{ A^{i}_{R}\, a^{i\dagger}_{\underline{q}} a^{i}_{\underline{q}} + B^{i}_{R} \left(a^{i\dagger}_{\underline{q}} a^{i\dagger}_{-\underline{q}} + a^{i}_{\underline{q}} a^{i}_{-\underline{q}} \right) \Big\} \\
& + \sum_{j} \Big\{ A^{j}_{T} b^{j\dagger}_{\underline{q}} b^{j}_{\underline{q}} + B^{j}_{T} \left(b^{j\dagger}_{\underline{q}} b^{j\dagger}_{-\underline{q}} + b^{j}_{\underline{q}} b^{j}_{-\underline{q}} \right) \Big\} \Bigg] + H' \qquad (7)
\end{aligned}
$$

where

$$
J^{ij}_{\alpha\beta}(\underline{q}) = \sum_{\underline{L}} J^{ij}_{\alpha\beta}(\underline{L}) \exp(-i\underline{q}\cdot(\underline{L}+\underline{d}^{i}_{\alpha}-\underline{d}^{j}_{\beta}))
$$

$\underline{L}$ is a lattice vector

H' is a $\underline{q}$ independent constant

and

$$
A^{i}_{R} = \frac{3S_2}{S_1} B^{o}_{2}(i) - \frac{30S_4}{S_1} B^{o}_{4}(i) + \frac{105S_6}{S_1} B^{o}_{6}(i) + \frac{21S_6}{S_1} B^{6}_{6}(i)
$$

$$
B^{i}_{R} = -\frac{3}{2}\sqrt{S_2}\, B^{o}_{2}(i) + \frac{15S_4}{\sqrt{S_2}} B^{o}_{4}(i) - \frac{105S_6}{2\sqrt{S_2}} B^{o}_{6}(i) + \frac{15S_6}{2\sqrt{S_2}} B^{6}_{6}(i)
$$

with

$$S_n = J_R(J_R-\tfrac{1}{2}).....\left(J_R - \frac{n-1}{2}\right).$$

The parameters describing the single ion anisotropy of the transition metal are (see Eq.(5))

$$A_T^i = 3(J_T-\tfrac{1}{2})\ B_2(i)$$

$$B_T^i = -\frac{3}{2}\sqrt{J_T(J_T-\tfrac{1}{2})} \cdot B_2(i) = -\frac{1}{2}\sqrt{J_T}\ A_T^i/\sqrt{J_T-\tfrac{1}{2}}$$

The expressions for A_k^i, B_R^i, A_T^i and B_T^i are valid only for a hexagonal system with an easy axis of magnetisation along the b-axis in the basal plane (see Fig. 6, p. 25).

2.3. The linear spin-wave solution

The time dependence of the magnon variables are given by the factor exp(-iωt) and the equations of motion by the commutator relation: (see Appendix C)

$$i\hbar\frac{d}{dt}\left(a_{\underline{q}}^i\, e^{-i\omega t}\right) = \left[a_{\underline{q}}^i\, e^{-i\omega t},\ H\right]$$

i.e.

$$\begin{aligned}
\hbar\omega\, a_{\underline{q}}^i &= [a_{\underline{q}}^i,\ H] \\
\hbar\omega\, a_{-\underline{q}}^{i\dagger} &= [a_{-\underline{q}}^{i\dagger},\ H] \\
\hbar\omega\, b_{-\underline{q}}^i &= [b_{-\underline{q}}^i,\ H] \\
\hbar\omega\, b_{\underline{q}}^{i\dagger} &= [b_{\underline{q}}^{i\dagger},\ H]
\end{aligned} \qquad (8)$$

where the Hamiltonian H is given by Eq.(7). The solution to the eigenvalue problem of Eq.(8) yields the magnon dispersion relations. The eigenvalues $|\hbar\omega|$ are the magnon energies and the different modes are described by the eigenvectors $a^i_{\underline{q}}$, $a^{i\dagger}_{-\underline{q}}$, $b^i_{-\underline{q}}$, $b^{i\dagger}_{\underline{q}}$. The actual number of equations in Eq.(8) is equal to two times the number of atoms in the unit cell. However, each solution is doubly degenerate, and the actual number of modes, or branches, in the dispersion relations equals the number of atoms in the unit cell.

For the mode described by $E = |\hbar\omega|$ and wave vector $\underline{q}$ the precession of the spins is given by: (Appendix C)

$$
\begin{aligned}
J_R^{ix}(\underline{\ell},t) &= \sqrt{\frac{2J_R}{N}}\left(a^i_{\underline{q}} + a^{i\dagger}_{-\underline{q}}\right)\cos\left(\underline{q}\cdot\underline{r}^i_R(\underline{\ell}) - \omega t\right)\\
J_R^{iy}(\underline{\ell},t) &= \sqrt{\frac{2J_R}{N}}\left(a^{i\dagger}_{-\underline{q}} - a^i_{\underline{q}}\right)\sin\left(\underline{q}\cdot\underline{r}^i_R(\underline{\ell}) - \omega t\right)\\
J_T^{jx}(\underline{m},t) &= \sqrt{\frac{2J_T}{N}}\left(b^j_{-\underline{q}} + b^{j\dagger}_{\underline{q}}\right)\cos\left(\underline{q}\cdot\underline{r}^j_T(\underline{m}) - \omega t\right)\\
J_T^{jy}(\underline{m},t) &= \sqrt{\frac{2J_T}{N}}\left(b^j_{-\underline{q}} - b^{j\dagger}_{\underline{q}}\right)\sin\left(\underline{q}\cdot\underline{r}^j_T(\underline{m}) - \omega t\right)
\end{aligned}
\qquad (9)
$$

The z-axis is the easy axis (see Fig. 20, p. 73), and as can be seen from Eq. (9), the precession of the spins is generally elliptic. This is an effect of the single ion anisotropy.

3. SPIN-WAVES IN Ho_2Co_{17} AND Ho_2Fe_{17}

After a short review of the crystallographic and static magnetic properties of the Ho_2Co_{17} and Ho_2Fe_{17} compounds, the experimental set-up is described, and the quality of the observed data is elucidated by a few examples. In Ho_2Co_{17} and Ho_2Fe_{17} only the low energy part of the magnon dispersion relations can be observed, and in Section 3.5 the general linear spin-wave model is simpli-

fied to cover only the experimentally observable range of energy transfers. In the last sections, the results of the least squares fit to the observed data, and the deduced exchange and crystal field parameters are presented.

Table 2. Site occupancy in disordered Ho_2Fe_{17} (Christensen and Hazell, 1980). The Wychoff notation has been used to identify the different sites.

Fe Site		Occupancy (%)	Ho Site		Occupancy (%)
Fe	4e	23	Ho	2b	--
Fe	4f	81	Ho	2d	100
Fe	6g	100	Ho	2c	20
Fe	12k	100			
Fe	12j	80			

Table 3. The lattice parameters (Christensen and Hazell, 1980), the average magnetic moment on the Ho and the transition metal sites (Laforest, 1966), and the ordering temperatures for Ho_2Co_{17} and Ho_2Fe_{17}. The free ion magnetic moment for Ho is 9.9 μ_B and the 3d magnetic moment in metallic Fe and Co is 2.2 μ_B and 1.7 μ_B (Betteridge, 1979).

COMPOUND	a (Å)	c (Å)	μ_R (μ_B)	μ_T (μ_B)	T_c (K)
Ho_2Co_{17}	8.322	8.113	9.0	1.6	1178
Ho_2Fe_{17}	8.458	8.282	9.9	2.1	335

3.1. Crystallographic and magnetic properties of Ho_2Co_{17} and Ho_2Fe_{17}

The crystal structure of Ho_2Co_{17} and Ho_2Fe_{17} is the complicated hexagonal Th_2Ni_{17} structure (Fig. 6), the space group is $P6_3/mmc$ and in the ideal case the unit cell contains two formula units, i.e. 38 atoms. A recent crystallographic examination of the

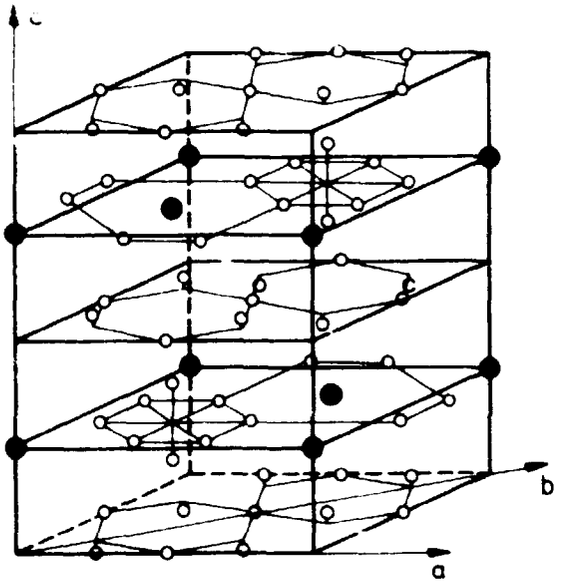

Fig. 6. The Th_2Ni_{17} structure. The filled circles are the rare earth ions, and the unfilled are the transition metal ions. In the figure, the crystallographic a, b, and c directions are defined.

single crystals used in this study (Christensen and Hazell, 1980) revealed that the structures were partly disordered, and Table 2 shows the occupancies of the different sites in Ho_2Fe_{17}. In the ideal Th_2Ni_{17} structure, the occupancy is 100% for all sites

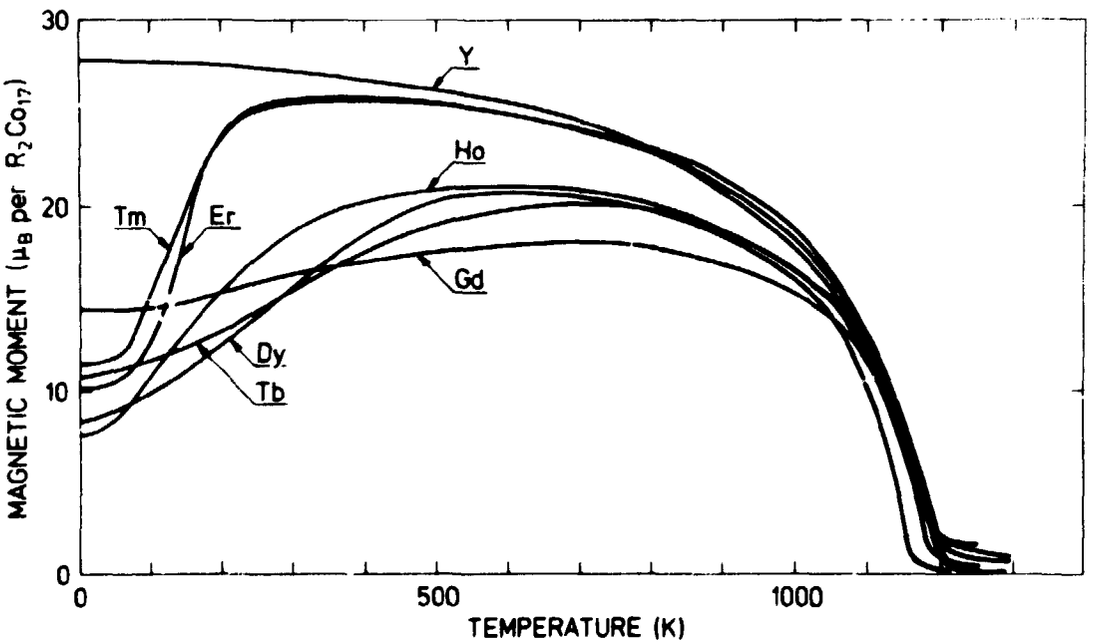

Fig. 7. The magnetisation curves for the ferrimagnetic R_2Co_{17} compounds, in units of Bohr magnetons per formula unit. In the figure only the rare earth ion defining the R_2Co_{17} compound has been marked. The data are from Laforest (1966).

except 2c and 4e, where it is zero. The structure analysis of Ho_2Co_{17} gave similar results, and in both cases a slight excess of Ho compared to the R_2T_{17} stoichiometry was observed (Christensen and Hazell, 1980).

Ho_2Co_{17} and Ho_2Fe_{17} are uniaxial ferrimagnets with the easy axis of magnetisation in the basal plane, along the b-axis (see Fig. 6), and in Table 3 the magnetic ordering temperatures, the average ordered magnetic moments of the two sublattices and the lattice parameters are quoted. In Fig. 7 the magnetisation curve for Ho_2Co_{17} is shown.

3.2. The Ho_2Fe_{17} and Ho_2Co_{17} samples

The Ho_2Co_{17} and Ho_2Fe_{17} single crystals were grown by A. Nørlund Chistensen (Christensen and Hazell, 1980) using Czochralski growth in a cold crucible. The samples were of almost cylindrical shape with the c-axis along the cylinder axis. The diameters of the samples were $\sim$ 6 mm and the length $\sim$ 12 mm (i.e. volume $\sim$ 0.34 cm^3). The Ho_2Co_{17} sample was one large single crystal. The Ho_2Fe_{17} sample contained one large and two smaller grains with a common c-axis, but where the small grains were rotated 6^o and 8^o around the c-axis with respect to the large grain. Samples from the same melt were prepared for the crystallographic studies (Christensen and Hazell, 1980) and for macroscopic anisotropy measurements (Clausen and Nielsen, 1981).

3.3. Experimental set-up

The neutron scattering experiments were performed using the triple-axis neutron spectrometers TAS I and TAS IV at the DR 3 steady-state reactor at Risø. Most of the experiments were performed using TAS I, which is a cold neutron spectrometer operating with a fixed incident energy. TAS IV is situated at a thermal beam, and this triple axis spectrometer was operated in the constant outgoing energy mode. In both cases pyrolytic graphite crystals were used for both analyser and monochromator, and a 2-inch py-

rolytic graphite filter was used, either after the monocromator (TAS I) or before the analyser (TAS IV) to reduce the higher-order contamination of the neutron beam. The beam was collimated in the horizontal scattering plane by means of vertical Cd-coated Soller slits. The details about the collimation and the neutron energies are given in Table 4.

Table 4. The collimation of the spectrometers is given in minutes of arc. R, M, S, A, D denotes reactor, monochromator, sample, analyser and detector, respectively. E_i is the fixed incident energy for TAS I and E_o is the fixed outgoing energy for TAS IV.

	Collimation				E_i	E_o
Spectrometer	R-M	M-S	S-A	A-D	(meV)	(meV)
TAS I	60'	56'	61'	66'	13.9	
TAS IV	58'	44'	54'	68'		13.9

In these experiments both constant-q and constant energy scans have been used. The neutron energy transfers were always measured for neutron energy loss, because all experiments were performed at low temperatures.

3.4. Experimental results

Before the actual results are shown, we will define our reciprocal lattice as a hexagonal coordinate system, where the angle between the positive directions of the basal plane unit vectors is 60°.

The inelastic neutron scattering studies of Ho_2Co_{17} and Ho_2Fe_{17} were performed at 4.2 K, and covered energy transfers between 1 and 28 meV, and $\underline{q}$ vectors along the three high-symmetry directions. The results are shown in Figs. 8 and 9. The open circles were observed around the (110) and (222) reciprocal lattice points, whereas the open squares were observed around the (200) point. Three different branches have been observed, a non-disper-

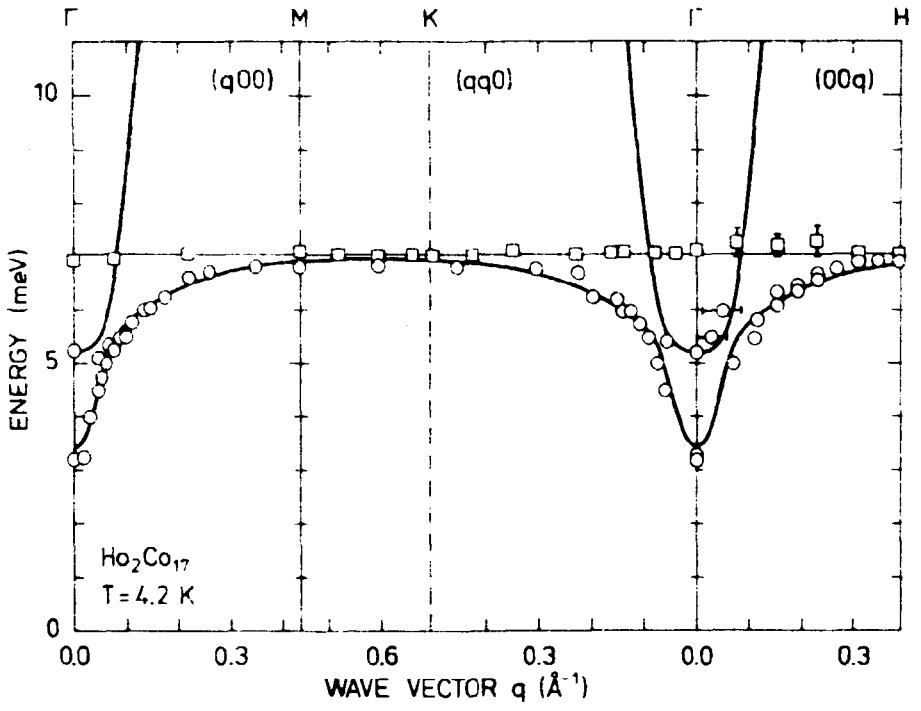

Fig. 8. The magnon dispersion relations in Ho_2Co_{17} at 4.2 K. The circles are observed around the (110) or (222) reciprocal lattice points, and the squares around the (200) point. The solid lines are the results of a fit to the linear spin-wave model as described in Section 3.5. The highly dispersive Co-mode could hardly be resolved from the much stronger rare earth mode in the range from 5-7 meV, and above 7 meV the Co-mode was too weak to be observed.

sive mode, a dispersive mode degenerate with the non-dispersive mode at the zone boundary, and a highly dispersive mode, i.e. both the number of observed modes, and the qualitative features of these modes are in exact agreement with the observed magnon dispersion relations in the cubic RT_2 compounds (Koon and Rhyne, 1979), and, as was the case for the cubic systems, the inelastic scattering from phonons was too weak to be observed.

In Figs. 10 and 11 constant q-scans at the zone centre are shown. The two dispersive modes are observed around the (110) reciprocal lattice point, where the dynamical structure factor for in-phase precession of the rare earth spins is maximum, and the non-dispersive - localised mode - with energy transfers of $E_{LOC}(Ho_2Fe_{17})$ = 8.3 meV and $E_{LOC}(Ho_2Co_{17})$ = 7.05 meV, were observed around the

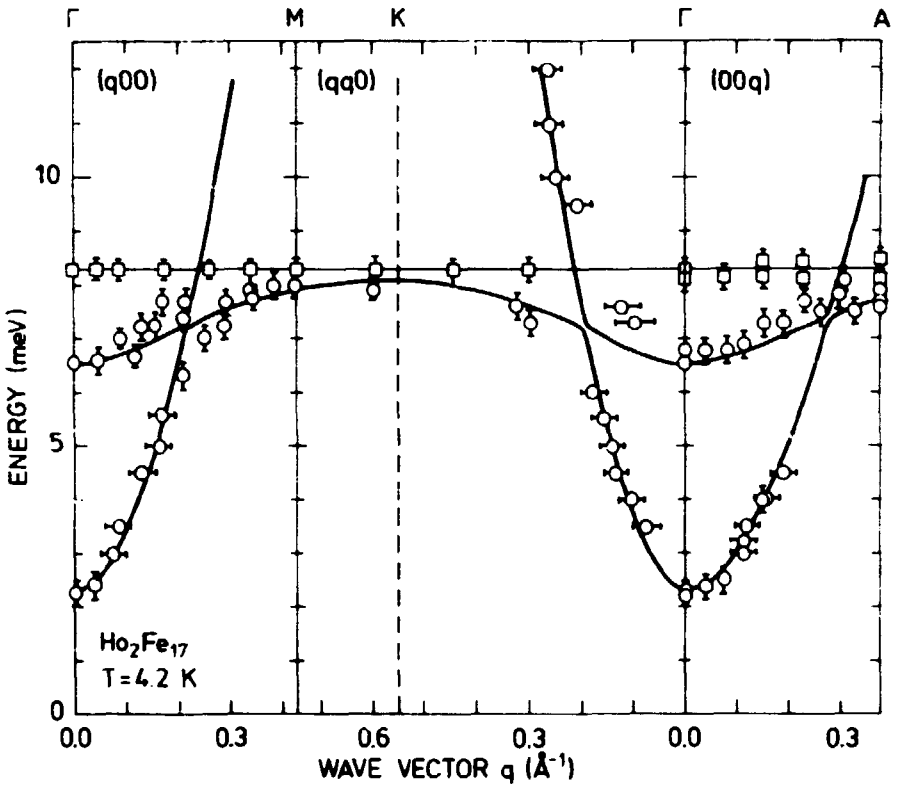

Fig. 9. The magnon dispersion relations in Ho_2Fe_{17} at 4.2 K. The circles are observed around the (110) or (222) reciprocal lattice points and the squares around the (200) point. The solid line is the result of a fit to the linear spin-wave model as described in Section 3.5. Because of the anisotropic Fe-Fe exchange, J_{Fe-Fe} takes different values in the different high-symmetry directions.

(200) point, where the dynamical structure factor for the rare earth sublattice is maximum for 180° out-of-phase precession. The highly dispersive modes, as observed in constant E scans are shown in Figs. 12 and 13. For energy transfers less than E_{LOC}, this mode can be observed both around the (110) and the (222) reciprocal lattice points, each of which is favourable for in-phase rare earth modes. For energy transfers above E_{LOC}, however, it is observed only for Ho_2Fe_{17}, and at the (222) reciprocal lattice point alone, where the dynamical structure factor for in-phase precession of the transition metal sublattice is large. The intensity of the highly dispersive Fe mode decreased rapidly as the corresponding energy transfers exceeded E_{LOC}. From the linear spin-wave model it was found that for energy transfers less than the energy of the localised mode, the highly dispersive mode was

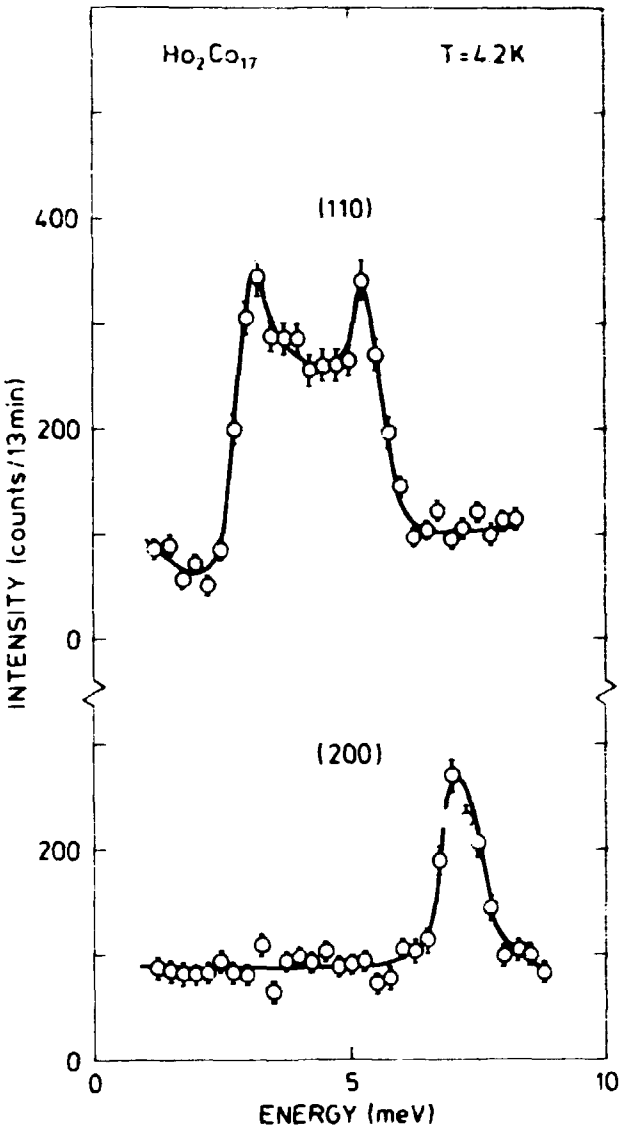

Fig. 10. The scattering observed at the zone centre in Ho_2Co_{17} at 4.2 K. Because of finite resolution, scattering from the highly dispersive Co-mode is observed in between the two peaks observed at the (110) reciprocal lattice point. Around the (200) point only the non-dispersive mode is observed. The solid lines are guides for the eye.

characterised by an in-phase precession of both the rare earth and transition metal sublattices, but the two sublattices were 180° out-of-phase (i.e. the local antiparallel coupling of the rare earth and the 3d-spins were preserved). Above E_{LOC} the precession of the rare earth sublattice died away rapidly. In a study of the cubic RCo_2 compounds Koon and Rhyne (1979) did not observe

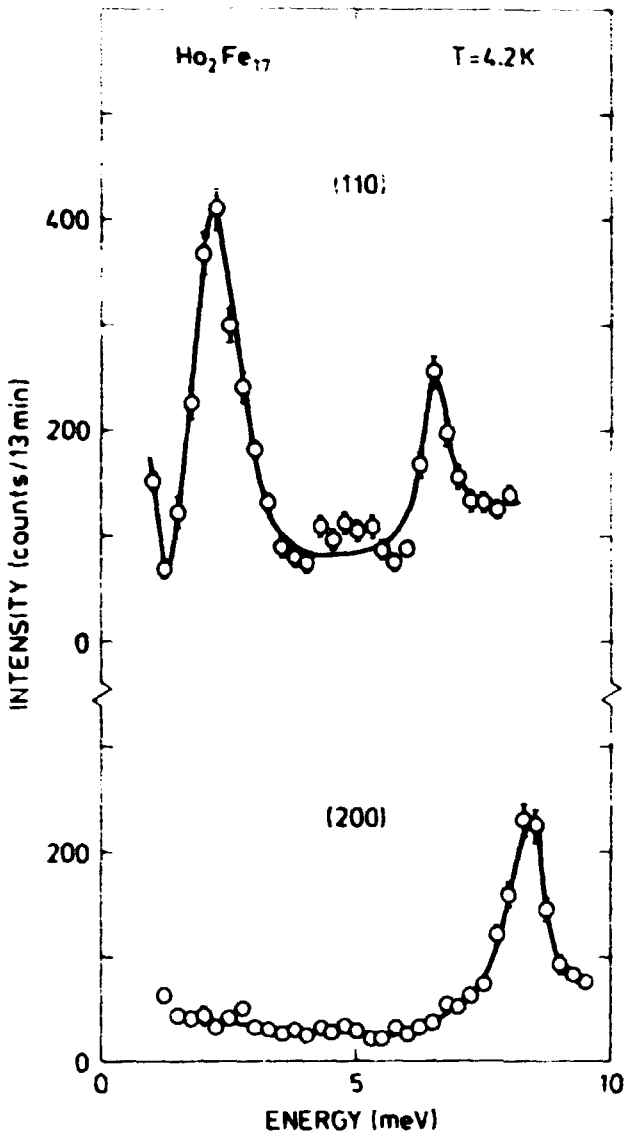

Fig. 11. The scattering observed at the zone centre in Ho_2Fe_{17} at 4.2 K. The two dispersive modes are observed at the (110) point and the localised mode around the (200) reciprocal lattice point. The solid lines are guides for the eye.

the highly dispersive Co mode and for some yet unknown reasons, modes which do not involve precession of the rare earth ions have never been observed in the R_nCo_m compounds. Also in this study the Co mode in Ho_2Co_{17} was not seen for energy transfers larger than E_{LOC}.

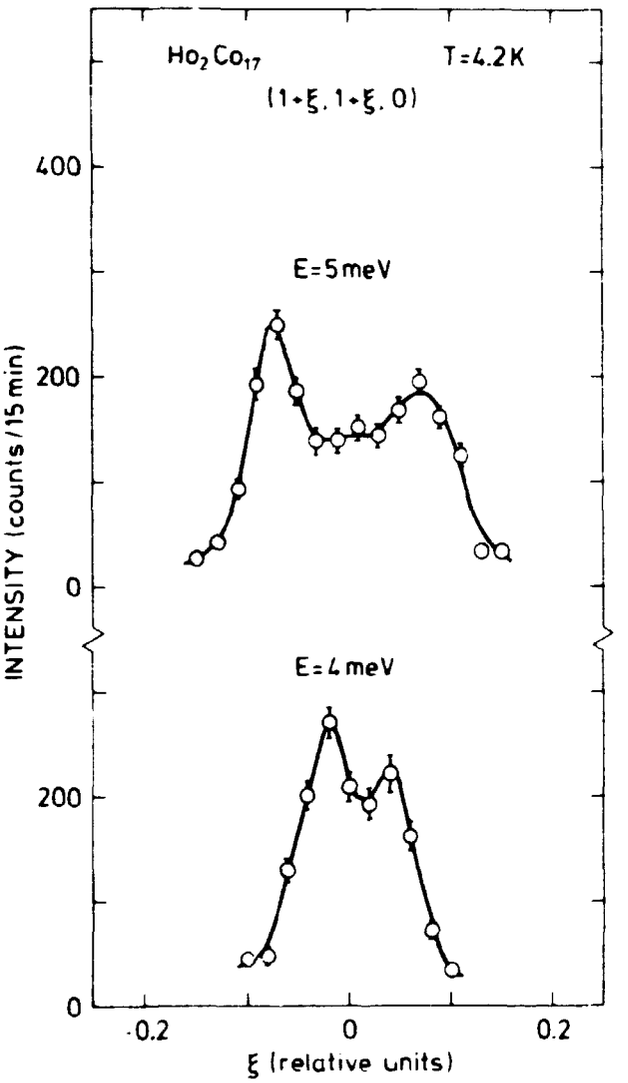

Fig. 12. Constant-E scans for the highly dispersive Co mode in Ho_2Co_{17} at 4.2 K. The difference in width and height for $\xi = q$ and $\xi = -q$ is a resolution effect. The solid lines are guides for the eye.

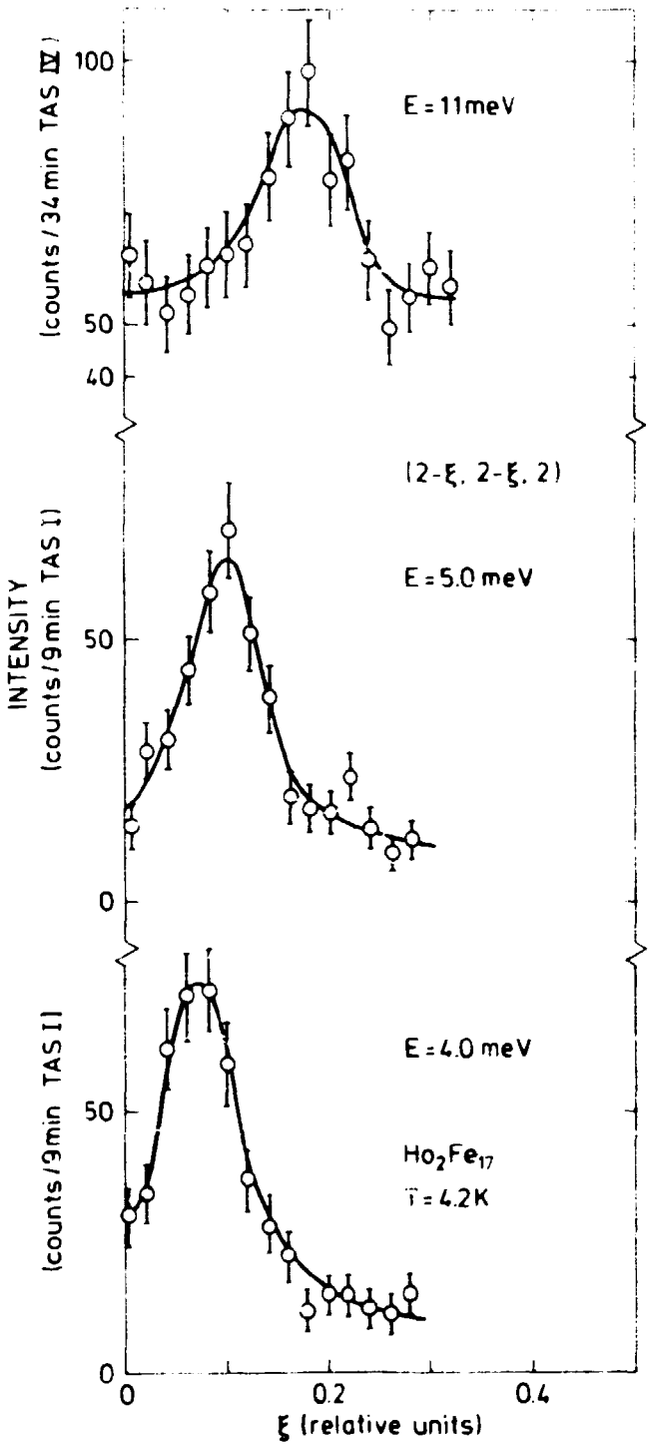

Fig. 13. Constant-E scans for the Fe-mode in Ho_2Fe_{17} at 4.2 K. The intensity of this mode decreases rapidly when the energy transfer exceeds 8 meV. The solid lines are guides for the eye.

3.5. Linear spin wave model for low energy magnons

The linear spin wave model (Section 2.3.) predicted one spin wave branch in the magnon dispersion relation per atom in the unit cell, i.e. for the ideal Th_2Ni_{17} structure, which will be assumed in the linear spin-wave model, 38 branches are predicted (4 modes corresponding to the 4 rare earth ions in the unit cell, and 34 from the 3d ions), but only three have been observed. In Fig. 14 we have sketched these three modes. The highly dispersive mode (solid line) has a parabolic shape. It is observed where

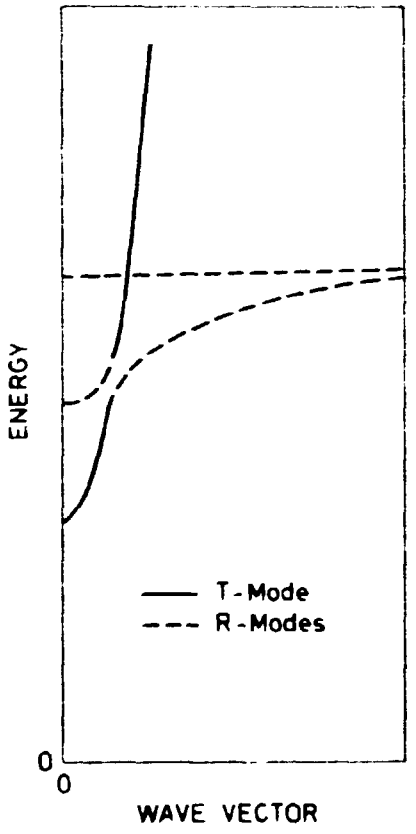

Fig. 14. Sketch of the observed low energy part of the magnon dispersion relations in R_2T_{17}. Because of their simple shape, the three dispersion curves can be described by six parameters, one gap and one dispersion parameter for each branch, i.e. only six parameters in a linear spin-wave model can be deduced from a fit to the observed data.

in-phase precession of the 3d-sublattice will give a large intensity, and it has a dispersion which is typical for a ferromagnetic transition metal. It is therefore interpreted as an in-phase transition metal mode, and in that case all the modes corresponding to the optical spin-waves in a pure transition metal will have energies much in excess of the practically achievable energy transfers in these experiments. Consequently only one

of the 34 modes corresponding to the number of 3d-ions in the unit cell can be observed. For the interpretation of the observed modes this means that the spin-wave Hamiltonian Eq.(7) can be greatly simplified because the magnon variables for the transition metal ions $b_{\underline{q}}^{i}$ and $b_{\underline{q}}^{i\dagger}$ are independent of i (the position of the 3d-ion in the unit cell). The model now predicts 5 modes, 4 modes corresponding to the 4 rare earth ions in the unit cell, and one from the 3d metal. The appearance of a non-dispersive mode can be explained only if the rare earth - rare earth exchange is negligible. Therefore, if we assume that $J_{RR}^{ij}(\underline{q}) = 0$, and furthermore, that the exchange and crystal field interactions of the two rare earth sites are identical, then three of the rare earth modes will be degenerate. This leads to only three non-degenerate observable modes. This means that when analysing the experimental results the parameters describing the exchange ($\sum_j J_{RT}^{ij}(\underline{q})$) and the crystal field interations (A_R^i and B_R^i) of the rare earth sublattice can be considered as independent of i (the rare earth position in the unit cell).

Using these approximations the linear spin wave model can be solved analytically (Appendix C) for the observed low energy branches. The result is:

$$(h\omega)^2 = a^2 - d_R^2 = E_{LOC}^2 \tag{10}$$

$$(h\omega)^2 = (a^2 - d_R^2 + b^2(\underline{q}) - d_T^2)/2 - N_R \cdot c^2(\underline{q})/N_T$$

$$\pm \sqrt{(a^2-d_R^2-b^2(\underline{q})+d_T^2)^2/4 - N_R \cdot c^2(\underline{q})((a+b(\underline{q}))^2-(d_R-d_T)^2)/N_T} \tag{11}$$

where Eq.(10) describes a triply degenerate non-dispersive mode, and Eq.(11) describes the two non-degenerate dispersive modes. The parameters in Eq.(10) and Eq.(11) are defined by the expressions:

$$a = A_R - 2J_T J_{RT}(\underline{0})/N_R$$

$$b(\underline{q}) = 2J_T\,(J_{TT}(\underline{q})-J_{TT}(\underline{0}))/N_T+2J_R J_{RT}(\underline{0})/N_T-\lambda_T$$

$$c(q) = -2\sqrt{J_R J_T}\; J_{RT}(\underline{q})/N_R$$

$$d_R = B_R$$

$$d_T = -B_T$$

J_R = total angular momentum for the rare earth ion

J_T = pseudo-spin for the transition metal ion (see Eq.(2))

N_R = number of rare earth ions in the unit cell

N_T = number of transition metal ions in the unit cell

$J_{\alpha\beta}(\underline{q}) = \sum_{ij\underline{L}} J^{ij}_{\alpha\beta}(\underline{L})\exp(-i\underline{q}\cdot(\underline{L}+\underline{d}^i_R-\underline{d}^j_T))$ is the Fourier transform of the exchange constant.

For Ho_2Fe_{17} and Ho_2Co_{17} the parameters describing the crystal field are given as

$$A_R = A_{HO} = 22.5\ B_2^0 - 10238\ B_4^0 + 1132431\ B_6^0 + 236486\ B_6^6 \qquad (11a)$$

$$B_R = B_{HO} = -11.62\ B_2^0 + 5287\ B_4^0 - 610605\ B_6^0 + 87229\ B_6^6$$

For the rare earth sublattice and

$$B_{Fe} = -0.69\ A_{Fe} = 1.15\ B_2(Fe) \qquad (11b)$$

$$B_{Co} = -0.80\ A_{Co} = 0.74\ B_2(Co)$$

For the transition metal sublattices see Eq.(5) for the definition of $B_2(T)$.

The experimental information about the 3d-metal is given mainly in one branch, the transition metal mode (Fig. 14), and hence only two parameters, J_{TT} and A_T, describing the 3d-3d exchange and the 3d-crystal field anisotropy, both averaged over the different transition metal sites, can be obtained. From the two rare earth modes (Fig. 14) four parameters describing the rare earth - rare earth and rare earth - transition metal interactions can be deduced. These four parameters are the two anisotropy parameters A_R, B_R and the two exchange parameters, J_{RR} and J_{RT}, where the last parameter represents an average over the different transition metal sites.

The Fourier transform of the exchange constants $J_{\alpha\beta}(\underline{q})$ can now be calculated using only one parameter in a nearest neighbour-like approach, where the exchange constant $J^{ij}_{\alpha\beta}(\underline{\ell},\underline{m})$ is given by

$$J^{ij}_{\alpha\beta}(\underline{\ell},\underline{m}) = \begin{cases} J_{\alpha\beta} & \text{for } |\underline{r}^i_\alpha(\underline{\ell}) - \underline{r}^j_\beta(\underline{m})| < 3 \text{ Å} \\ 0.0 & \text{otherwise} \end{cases} \qquad (12)$$

In this way the exchange is assumed to be between one ion and all the directly contacting surrounding ions. In this approximation the exchange is taken to be independent of the ion-ion separation, which is not supposed to hold for the Fe compounds. (See the Bethe-Slater curve Fig. 5). Using the limit of 3 Å in Eq. (12) automatically means that $J_{RR}(\underline{q}) = 0$ because the rare earth - rare earth separation is greater than 4 Å.

In the R_2T_{17} compounds $J_{\alpha\beta}(\underline{q})$ can be calculated from the knowledge of the crystal structure discussed in Section 3.1.

For $\underline{q} = (\xi,0,0)$

$$J_{RT}(\xi) = J_{RT}(12.6 + 28.8 \cos(2\pi\xi/3) + 32 \cos(2\pi\xi/6))$$

$$J_{TT}(\xi) = J_{TT}(80 + 176 \cos(2\pi\xi/6) + 96 \cos(2\pi\xi/3))$$

For $\underline{q} = (\xi,\xi,0)$

$$J_{RT}(\xi) = J_{RT}(22.2 + 12.8\cos(2\pi\xi/3) + 6.4\cos(4\pi\xi/3) + 32\cos(\pi\xi))$$

$$J_{TT}(\xi) = J_{TT}(44 + 96\cos(2\pi\xi/6) + 104\cos(2\pi\xi/3) + 80\cos(2\pi\xi/2) + 28\cos(4\pi\xi/3))$$

and for the third high symmetry direction:
$\underline{q} = (0,0,\xi)$

$$J_{RT}(\xi) = J_{RT}(19.2 + 43\cos(2\pi\xi/4) + 6.2\cos(2\pi\xi 0.36)$$

$$J_{TT}(\xi) = J_{TT}(108 + 48\cos(0.22\pi\xi) + 48\cos(0.28\pi\xi) + 144\cos(\tfrac{1}{2}\pi\xi + 4\cos(0.56\pi\xi))$$

3.6. Least squares fitting procedure

From the observed three spin wave branches only six parameters can be deduced, and in the preceding section they were identified as the three nearest neighbour exchange constants, J_{RR}, J_{RT}, and J_{TT}, and the two parameters describing the crystal field interactions of the rare earth ion, A_R and B_R, and one parameter describing the 3d-crystal field, A_T. However, from the non-dispersive, localised mode one parameter and one constraint can be deduced:

$$J_{RR} = 0$$

$$E_{LOC}^2 = (A_R^2 - 2J_T\, J_{RT}(\underline{0})/N_P)^2 - B_R^2$$

where E_{LOC} is the energy transfer observed for the localised mode, and the constraint is taken from the spin wave solution Eq.(10). We are now left with four free parameters. These parameters have been determined using a general least squares fitting procedure, to fit the observed data from the two dispersive modes

to the calculated dispersion relation Eq.(11), for one high symmetry direction at a time. In Table 5 the input parameters for the fits are shown.

Table 5. The input parameters used in the fit to the linear spin-wave model. The parameters are defined in connection with Eq.(11).

Compound	E_{LOC} (meV)	J_{RR} (meV)	B_T/A_T	N_R	N_T	J_R	J_T
Ho_2Co_{17}	7.05	0.0	-0.816	4	34	8.0	0.8
Ho_2Fe_{17}	8.30	0.0	-0.691	4	34	8.0	1.05

3.7. Spin-wave results

For Ho_2Co_{17} the parameters obtained from the fits were consistent for the three different high symmetry directions and the deduced parameters are quoted in Table 6. The resulting dispersion relations are shown as the solid lines in Fig. 8.

Table 6. The final parameters deduced from the fits to the linear spin-wave model for Ho_2Co_{17} and Ho_2Fe_{17}. The uncertainties of the parameters are estimated within the model used, i.e. systematic errors caused by inadequacies of the model used are not taken into account.

Compound	A_R (meV)	B_R (meV)	J_{RT} (meV)	J_{TT} (meV)	A_T (meV)	B_T (meV)
Ho_2Co_{17}	2.88±0.15	-0.26±0.20	-0.14±0.01	21.8±2.0	0.61±0.15	-0.50±0.22
Ho_2Fe_{17}	3.74±0.20	-0.33±1.00	-0.12±0.02	Anisotropy	0.0 ±0.50	0.0 ±0.35

For Ho_2Fe_{17} the four parameters in the linear spin-wave fits were highly correlated, and the results for the different symmetry directions were inconsistent. Because the spin-wave anisotropy parameter A_{Fe} always came out with a value close to zero (with a rather large error bar), A_T was fixed at zero in the

final fits. In this way consistent results for A_R, B_R and J_{RT} were obtained (see Table 6), but J_{Fe-Fe} still deviated substantially for the different directions (see Table 7). Figure 9 shows the observed data and the spin-wave dispersion relations for Ho_2Fe_{17} (solid lines) with an Fe-Fe exchange constant that differs for the different directions. In Table 7 we have included the observed ordering temperature T_c, and the mean field ordering temperature, calculated from the exchange constant using Eq.(3). In both cases the agreement is good.

Table 7. The final parameters for the 3d-3d exchange in the different high symmetry directions, the mean field ordering temperature calculated from the exchange constants, and the observed ordering temperatures taken from Laforest (1966) and Gubbens (1977).

Compound	J_{TT}(meV) (ξ00)	(ξξ0)	(00ξ)	T_c^{MF}(K)	T_c^{OBS}(K)
Ho_2Co_{17}	23.4±1.9	18.8±2.0	23.2±2.7	1257±115	1178
Ho_2Fe_{17}	3.48±0.34	4.52±0.28	2.45±0.30	301±103	335

In Fig. 15 the dispersion of the transition metal mode in the different directions for Ho_2Co_{17} and Ho_2Fe_{17} are compared. The apparent anisotropy of the Fe-Fe exchange and the isotropic character of the Co-Co exchange can be qualitatively understood with the aid of the Bethe-Slater curve (Fig. 5), and the fact that Ho_2Co_{17} and Ho_2Fe_{17} are closed packed like structures, which have been compressed slightly along the c-axis so that the 3d-3d separation is generally shorter in the out-of-plane direction than within the basal plane. In Ho_2Fe_{17}, J_{FeFe} is very sensitive to the interatomic Fe-Fe distance, and, as observed, we would expect the Fe-Fe exchange to be smallest in the [00ξ] direction. For Ho_2Co_{17}, J_{CoCo} lies close to a flat maximum of the Bethe-Slater curve, and hence we would expect the observed isotropic behaviour.

The parameter $B_2(T)$ describing the crystal field anisotropy of the transition metal (Eq.(5)) and the crystal field parameters

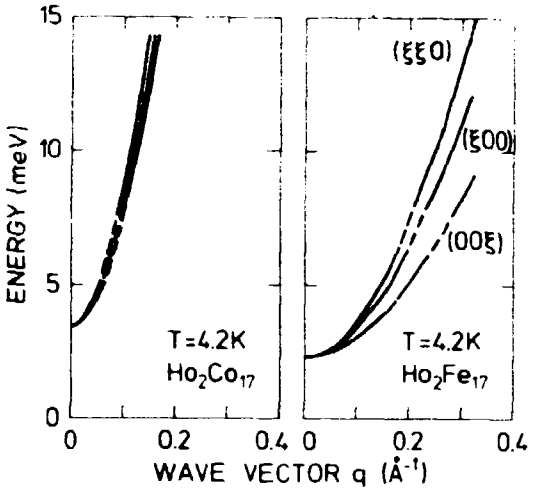

Fig. 15. The dispersion of the transition metal modes in Ho_2Co_{17} and Ho_2Fe_{17} at 4.2 K. The lines are dotted in the region where the two dispersive modes mix. In Ho_2Co_{17} the differences in the observed dispersion is within the experimental error, whereas in Ho_2Fe_{17} the anisotropy of the 3d-3d exchange is evident.

$B_2^0(R)$, $B_6^6(R)$ can be calculated from A_T, A_R and B_R using Eq.(11a) and Eq.(11b) if $B_4^0(R)$ and $B_6^0(R)$ are assumed to be negligible. The results are quoted in Table 8. $B_2^0(Ho)$ and $B_6^6(Ho)$ are slightly larger in Ho_2Fe_{17} than in Ho_2Co_{17}, but the difference is not significant (the two sets of parameters agree within the experimental uncertainty), and the sign of $B_2^0(Ho)$ and $B_6^6(Ho)$ is, of course, in agreement with the observed easy b-axis. Creedan and Rao (1973) have estimated the crystal field parameter $B_2^0(Ho)$ for the two Ho sites in Ho_2Co_{17} using a point charge model and neglecting the influence of the Co ions. They obtained values for $B_2^0(Ho)$ which are of the same order of magnitude as our results,

Table 8. The crystal field parameters for Ho_2Co_{17} and Ho_2Fe_{17} as derived from the spin-wave fit, and as calculated from a point charge model neglecting the influence of the Co sublattice (Credan and Rao, 1973). In the point charge calculations the contribution from the two rare earth sites 2b and 2d (Wyckoff notation) are different.

	Point charge R-only		This study		
	site 2b	site 2d	R-sites		T-sites
	B_2^0 (meV)	B_2^0 (meV)	B_2^0 (meV)	B_6^6 (10^{-6}meV)	B_2 (meV)
Ho_2Co_{17}	0.060	-0.045	0.066±0.010	5.88±1.20	0.68±0.30
Ho_2Fe_{17}			0.086±0.054	7.63±5.27	0.0±0.30

but according to their results, the two Ho sites should display very different anisotropic behaviour, because the sign of B_2^0(Ho) should be different (Table 8). We, however, feel that the Co ions should not be neglected, and find our assumption of identical exchange and crystal field interactions of the two rare earth sites to be plausible because:

a) Only three modes were observed. If the two sites were different, five modes should have been observed.

b) The two sites have the same point symmetry.

c) 18 out of 20 nearest neighbours are in equivalent relative positions to the two sites.

d) If the observed disorder of the compounds is taken into account, one cannot on the average distinguish between the nearest neighbour surroundings of the two sites.

Using our linear spin-wave model, the low energy part of the observed magnon dispersion relations for Ho_2Co_{17} and Ho_2Fe_{17} can be reproduced, and at first sight the parameters deduced from the fit to the linear spin-wave model yield the correct signs and orders of magnitude. In the next chapter the adequacy of the model will be more thoroughly tested by using the deduced parameters to predict independently observed magnetic properties of Ho_2Co_{17} and Ho_2Fe_{17}.

4. MAGNETIC PROPERTIES PREDICTED BY THE PARAMETERS DEDUCED FROM THE SPIN WAVE FIT

The linear spin wave model used to analyse the observed data is based on many simplifying assumptions (see Chapter 3). The 3d-magnetic moment has been treated as pseudo spins interacting via the isotropic nearest neighbour exchange and the single ion

crystal field interactions. In the present approximation we have assumed that the 3d-sites could be considered as one single site with average parameters for the pseudo-spins $J_T = \mu_T/2\mu_B$, the exchange constant and the crystalline electric field.

Especially for Ho_2Fe_{17} the rather low ordering temperature and the neglect of the two ion anisotropy is rather crude, but as the inelastic neutron scattering data shows only three branches of very simple shape, it would be highly dubious to introduce more variables. The degree of confidence in the simple approach that has been adapted in this thesis is therefore closely related to the ability to predict other independently observable magnetic properties by means of the deduced parameters. In the following paragraphs the spin wave parameters are tested against the observed temperature dependence of the localised mode, macroscopic anisotropy parameters, and in the case of Ho_2Co_{17}, with the magnetization curve.

4.1. Temperature dependence of the localised mode

For the non-dispersive modes (10) it is a good approximation to regard the rare earth spins as independent spins situated in a molecular field from the transition metal spins and in a crystal field originating from the surrounding ions. The single ion Hamiltonian describing this situation is given by:

$$\begin{aligned} H_{MF} &= H_{CF} - \underline{\mu}\cdot\underline{B} \\ &= H_{CF} + g\,\mu_B\,\underline{B}\cdot\underline{J}_R \end{aligned} \qquad (14)$$

where

$$H_{CF} \simeq B_2^0\,O_2^0 + B_6^6\,O_6^6$$

$$g\,\mu_B\,\underline{B} = -2 \sum_{j\underline{\ell}} J_{RT}^{ij}(\underline{\ell})\;\underline{J}_T^j(\underline{\ell})$$

$$= - \frac{2}{N_R} J_{RT}(\underline{0}) \; \underline{J}_T$$

Here the crystal field Hamiltonian is given in the c-axis representation and B_4^0 and B_6^0 are assumed to be negligible. The direction of $\underline{J}_T$ is along the b-axis (see Fig. 6).

In the independent dipole approximation the intensity of the scattering from this mode at a given temperature T - including instrumental resolution - can be calculated as (de Gennes, 1963):

$$I(\omega,T) = \sum_{if} \left\{ \rho_i \, | \langle f | \hat{J}_\perp | i \rangle |^2 \, k_i/k_f \right.$$

$$\left. * C \exp(-(\hbar\omega - E_j + E_i)^2/\sigma_{if}^2) \right\} + B \qquad (15)$$

where

- C is a normalising constant
- $\hat{J}_\perp$ is the component of the momentum operator perpendicular to the scattering vector $\underline{\kappa} = \underline{k}_i - \underline{k}_f$
- $\underline{k}_i, \underline{k}_f$ are the initial and final wave vectors
- σ_{if} is the energy resolution width of the spectrometer for an energy transfer of $E_i - E_f$
- ρ_i is the Boltzmann population factor for the initial state
- B is a constant background.

The initial and final energies E_i, E_f and wave functions $\langle i|$, $\langle f|$ are determined by diagonalisation of the mean field Hamiltonian Eq. (14)

$$H_{MF} \, |n\rangle = E_n \, |n\rangle$$

where n = i or f.

In the right hand sides of Figs. 16 and 17 the level schemes, transition probabilities $|\langle f|\hat{J}_\perp|i\rangle|^2$ between adjacent states and

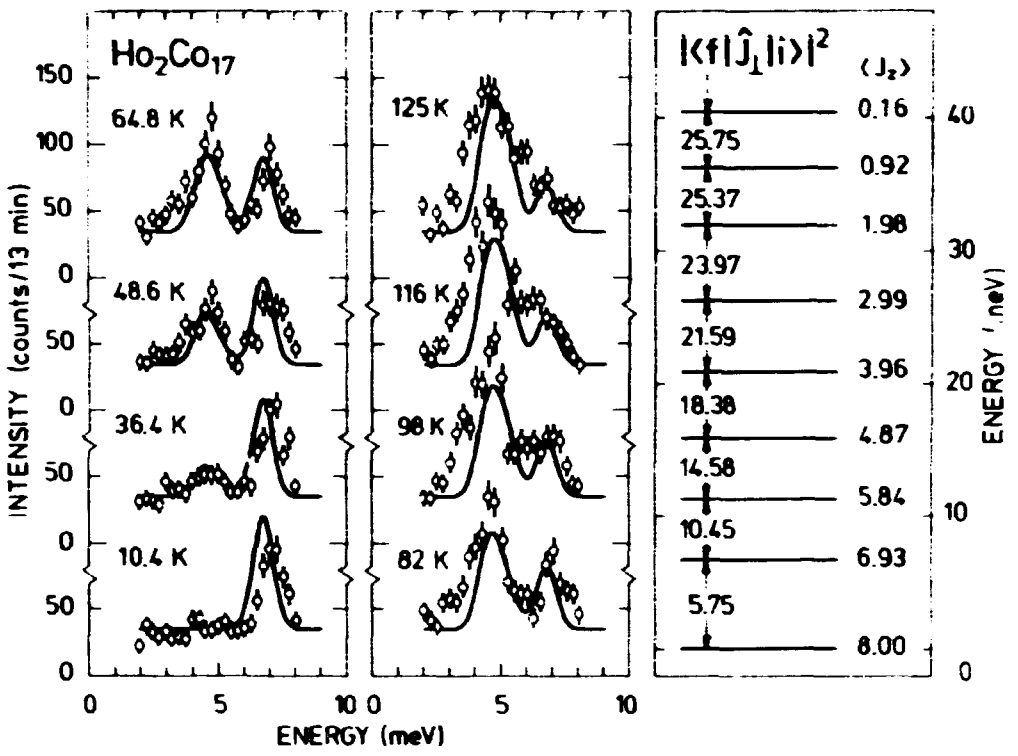

Fig. 16. The scattering from the localised (non-dispersive) mode in Ho_2Co_{17} at different temperatures. The solid curves are calculated from a mean field model using the parameters deduced from the fit to the linear spin-wave model. The energy levels, the z-component of the total angular momentum J_z, and the transition probabilities within the mean field model are given in the right part of the figure. The line shape of the scattered intensity is calculated using the known energy resolution of the spectrometer.

the component of the total angular momentum of the Ho ions along the quantisation axis are shown for Ho_2Co_{17} and Ho_2Fe_{17}. Almost pure J_z states were found in both cases, and calculations show that the transition probabilities between non-adjacent states are about two orders of magnitude lower than for adjacent state transitions, and have therefore been neglected in the analysis. The solid lines in the left-hand sides of Figs. 16 and 17 are the calculated scattering from the non-dispersive mode at different temperatures, using Eq.(15), and the open circles are the observed scattering. In the calculations, the background B was taken from the experiment as the observed scattering outside the regions of the peaks. The normalisation constant was esti-

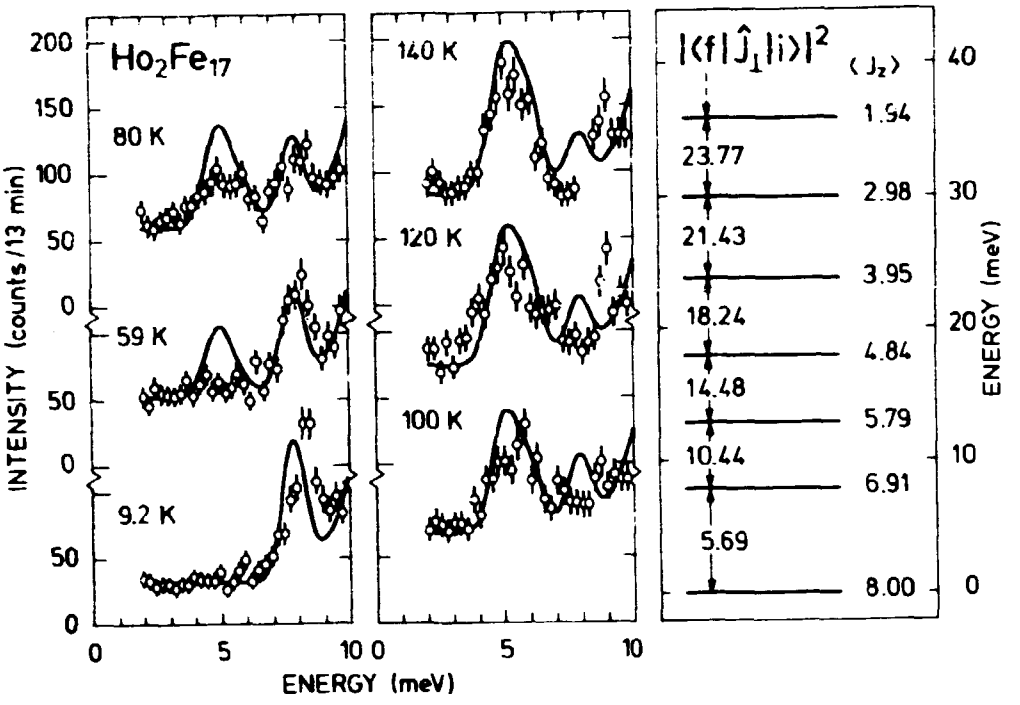

Fig. 17. The temperature dependence of the scattering from the localised (non-dispersive) mode in Ho_2Fe_{17}. The solid curves are the result of a mean field calculation. (See the figure caption for Fig. 16).

mated by inspection, and kept temperature invariant. The rest of the parameters in the calculations are given by the paramenters deduced from the spin-wave fits and the resolution of the spectrometer.

For Ho_2Co_{17}, the agreement between the observed and calculated scattering is remarkably good (see Fig. 16). For Ho_2Fe_{17} the peak at approximately 5 meV starts developing at a too low temperature, and the peak at $\sim$8 meV dies out too slowly, but nevertheless, the general features are correct, and, as mentioned before, the approximations made in the linear spin-wave model are much more severe for the Ho_2Fe_{17} than for the Ho_2Co_{17} compound.

4.2. Macroscopic anisotropy constants

The macroscopic free energy of a magnetic system can be calculated from the microscopic Hamiltonian by the equation (Lindgård and Danielsen, 1975)

$$F(\theta,\phi) = - k_B T \ln \left(\sum_i \exp(-E_i(\theta,\phi)/k_B T)\right) \qquad (16)$$

where E_i is given by $H(\theta,\phi)|i\rangle = E_i(\theta,\phi)|i\rangle$, k_B is Boltzmann's constant, and $H(\theta,\phi)$ is the Hamiltonian in a representation in which the direction of the quantization axis is given by the polar coordinates θ and ϕ. θ is the angle of the magnetisation relative to the hexagonal axis, and ϕ is the angle in the basal plane relative to the a-axis (see Fig. 6).

For hexagonal symmetry the free energy in Eq.(16) is generally assumed to take the form

$$F(\theta,\phi) = k_o(T) + k_1(T) \sin^2\theta + k_2(T) \sin^4(\theta) + k_3(T) \sin^6\theta + k_4(T) \sin^6\theta \cos 6\phi \qquad (17)$$

where $k_n(T)$ are the macroscopic anisotropy constants. At low temperatures only the ground state contributes to the free energy, and Eq.(16) can be rewritten as

$$F(\theta,\phi) = E_o(\theta,\phi) = E_{ex} + E_{CF}(\theta,\phi)$$

where E_{ex} is θ and ϕ independent if:

a) the exchange is isotropic and

b) the exchange is sufficiently strong to preserve colinearity.

$E_{CF}(\theta,\phi)$ takes the form of the crystal field Hamiltonian, but the spin operators are interpreted as clasical spins. If we assume $B_4^o = B_6^o = 0$ the $E_{CF}(\theta,\phi)$ per formula unit is

$$E_{CF}(\theta,\phi)/N = 2\ (B_2^0(R)O_2^0(R) + B_6^6(R)O_6^6(R))$$

$$+ 17\ B_2(T)\ [3(J_T^z)^2 - J_T(J_T+1)]$$

$$= 2\ B_2^0(R)\ [3(J_R^z)^2 - J_R(J_R+1)] + B_6^6[(J_R^+)^6 + (J_R^-)^6]$$

$$+ 17\ B_2(T)\ [3(J_T^z)^2 - J_T(J_T+1)]$$

using

$$J_\alpha^x = J_\alpha \sin\theta \cos\phi$$

$$J_\alpha^y = J_\alpha \sin\theta \sin\phi$$

$$J_\alpha^z = J_\alpha \cos\theta$$

$$J_\alpha^+ = J_\alpha^x + i\ J_\alpha^y = \sin\theta \exp(+i\phi)$$

$$J_\alpha^- = J_\alpha^x - i\ J_\alpha^y = \sin\theta \exp(-i\phi)$$

$$E_{CF}(\theta,\phi) = N\left(E_o - (6B_2^0(R)\ J_R^2 + 51\ B_2(T)\ J_T^2)\sin^2\theta\right.$$

$$\left. + 2\ B_6^6\ J_R^6 \sin^6\theta \cos 6\phi\right) \qquad (17)$$

where N is the number of formula units in the system.

From a direct comparison of Eq.(16) and Eq.(17) we find

$$K_1(T) = N\ (6\ B_2^0(R)\ J_R^2 + 51\ B_2(T)\ J_T^2)$$

$$K_4(T) = 2\ N\ B_6^6\ J_R^6 \qquad (18)$$

In Table 9 we have quoted the anisotropy constants as calculated from Eq.(18) using the crystal field parameters deduced from the spin wave fit, and as observed from magnetisation measurements (Clausen and Nielsen, 1981).

Table 9. The magnetic anisotropy constants K_1 and K_4 for Ho_2Co_{17} and Ho_2Fe_{17} at a temperature of 4.2 K. K_1^{OBS} and K_4^{OBS} are the experimentally observed quantities (Clausen and Nielsen, 1981). For Ho_2Fe_{17} the hard axis magnetization curve could only be explained if the higher order anisotropy constant K_2 was included. K_1^{CALC} and K_4^{CALC} are calculated from the crystal field parameters deduced from the spin-wave fit. K_1^{CALC} is quoted for both the situation where the transition metal is neglected (R-only) and the case where contributions from both sublattices are taken into account.

Compound	K_1^{CALC} (10^7 erg/cm^3)	K_1^{CALC} R-only (10^7 erg/cm^3)	K_1^{OBS} (10^7 erg/cm^3)	K_4^{CALC} (10^7 erg/cm^3)	K_4^{OBS} (10^7 erg/cm^3)
Ho_2Co_{17}	-30.9 ± 8.9	-16.4 ± 2.5	-1.48 ± 0.04	2.0 ± 0.4	0.066 ± 0.002
Ho_2Fe_{17}	-20.6 ± 23.6	-20.6 ± 13.0	-5.65 ± 0.05 (K_2 = 1.75 ± 0.05)	2.5 ± 1.5	0.085 ± 0.003

If the rare earth contribution to the anisotropy alone is taken into account, the calculations for Ho_2Co_{17} overestimates $K_1(T)$ by a factor of ∿11 and $K_4(T)$ by a factor of ∿32. Inclusion of the transition metal contribution makes the agreement even worse. For Ho_2Fe_{17} the magnetization data shows that the higher order axial anisotropy terms (B_4^o) cannot be neglected.

4.3. The magnetisation curve for Ho_2Co_{17}

For the R_2Co_{17} compounds the ordering temperature T_c and the magnetic moment of the Co ions μ_{Co} are almost independent of the rare earth ion R, and the temperature dependence of μ_{Co} can be found from

$$\mu_{Y_2Co_{17}}(T) = 17\ \mu_{Co}(T)$$

$$= 34\ \mu_B\ J_{Co}(T)$$

where we have used the definition of the pseudo-spin $\underline{\mu}_T = -2\mu_B \underline{J}_T$.

Within mean field theory the thermal average of the total angular momentum $\langle J_R \rangle$ of the rare earth ions can be calculated from the mean field Hamiltonian (14) using

$$\langle J_R \rangle = \sum_i \langle i|J_z|i\rangle \exp(-\beta E_i)/\sum_i \exp(-\beta E_i)$$

where

$$\beta = k_B T \text{ and } E_i = \langle i|H_{MF}|i\rangle$$

The magnetisation curve for Ho_2Co_{17} is then given as

$$\mu_{Ho_2Co_{17}} = \mu_{Y_2Co_{17}} - 2\, g_{Ho}\, \mu_B \langle J_{Ho}\rangle$$

where $g_{Ho} = 1.25$ and $\mu_{Y_2Co_{17}}$ is taken from experiment (Laforest, 1966). In Fig. 18 the solid line shows the observed magnetisation curves for Y_2Co_{17} and Ho_2Co_{17} (Laforest, 1966) and the open cir-

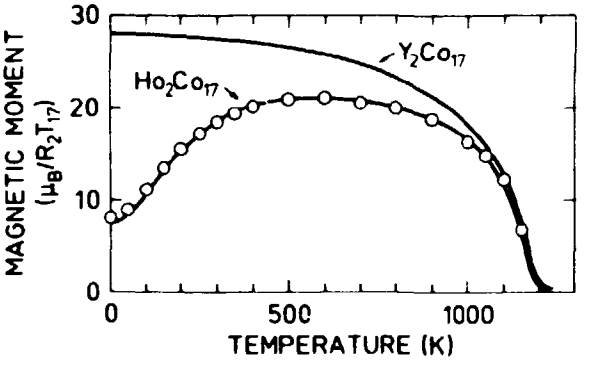

Fig. 18. The magnetisation curves for Ho_2Co_{17} and Y_2Co_{17}. The solid lines represent experimental results by Laforest (1966) and the circles are calculated from a mean field model using the parameters deduced from the fit to the linear spin-wave model.

cles are calculated using the parameters from the spin-wave fit and the observed magnetisation for Y_2Co_{17}. The agreement is excellent at all temperatures, which means that the deduced rare earth - transition metal exchange constant J_{RT} yields a good description of coupling between the two sublattices.

5. DISCUSSION

In this Chapter we first describe the present understanding of the general magnetic properties of the transition metal rich R_nT_m compounds. Then the used phenomenological model and its limitations are discussed, and finally the conclusions drawn from the experimental observations are reviewed.

5.1. General magnetic properties of R_2T_{17} compounds

First principle calculations of the magnetic properties have so far shown impossible, and the present phenomenological theories of magnetism can generally be divided into two main groups: a) the localized theories for the rare earth metals where the magnetic interactions in the solid only result in small perturbations of the free ion 4f wave-functions (i.e. the 4f electrons can be considered as residing permanently on a given ion), and b) the itinerant energy band theory of magnetism where the electrons are considered as belonging to the whole crystal rather than to the individual ions, and where the magnetic ground state is heavily influenced by the lattice (e.g. 3d electrons in the transition metals). At present no simple theories combining these two extreme cases are available.

The transition metal rich R_nT_m compounds can be considered as consisting of two weakly interacting subsystems, because the rare earth 4f wave functions and the transition metal 3d band is only slightly affected on forming the compounds. The main effects of the rare earth ions on the 3d ions are the decrease in the 3d coordination number of the transition metal sites, and the change in the electronic properties of the transition metal that results from the distortions of the local symmetry of the 3d ions produced by the mere presence of the rare earth ions. The main effect of the transition metal sublattice on the rare earth ions is to provide a large molecular field at the rare earth sites, and a charge distribution leading to a crystalline electric field

Both the 4f and the 3d electrons will of course interact with the conduction electrons, and the quenching of the RKKY type rare earth - rare earth exchange interactions is presumably caused by the dominance of the interactions between the 3d electrons and the conduction band.

The rare earth and the transition metal sublattices thus forms two very different subsystems and apart from the zone centre part of the "acoustic" (inphase) transition metal mode, the excitation spectra of the two subsystems are found in two well separated ranges of energy transfers. In the present experiments only the low energy part (<20 meV) of the excitation spectrum could be observed, i.e. only the rare earth modes, and the zone centre part of the acoustic 3d-mode have been observed and hence the amount of information about the interactions between the 3d ions will be limited to the gross features. This acoustic 3d mode only displays the magnetic properties averaged over the different transition metal sites. The 3d sublattice of the R_2T_{17} compounds is known to show a simple ferromagnetic ordering scheme, but apart from that, the magnetic properties of the 34 3d ions in the unit cell, distributed over 4-5 sites of different point symmetry are quite complex. A polarized neutron diffraction study of Lu_2Fe_{17} (Givord 1976) revealed that the magnetic moments on the different Fe sites varied from 1.9 ± 0.15 μ_B to 2.85 ± 0.20 μ_B. The hyperfine field on the Fe sites in Tb_2Fe_{17} (Gubbens 1977) determined by Mössbauer spectroscopy were found to vary from 26.2 T to 36.7 T (in the Co compounds the difference between the hyperfine field and the magnetic moments on the different Co sites is assumed to be much smaller), and in an NMR study of Y_2Co_{17} the anisotropy of the different Co sites (Streever 1978) varied from sites weakly favouring an easy c-axis to sites strongly favouring an easy basal plane. However, since the difference between the 3d sites is only displayed in the optic transition metal modes, which could not be observed in this experiment, we are only able to derive average exchange and crystal field parameters for the transition metal sublattice.

5.2. Phenomenological model

The low energy part of the magnon dispersion relations of Ho_2Fe_{17} and Ho_2Co_{17} is dominated by the rare earth contributions and we have chosen a localized (rare earth) description of the magnetic interactions, with a Hamiltonian including isotropic exchange and single ion anisotropy. The parameters describing the exchange and the crystal field anisotropy exhausts the number of parameters that can be deduced from a linear spin-wave interpretation of the experimental results, and hence less important interactions, such as for instance magnetostriction, are neglected. Localized models are of course generally inadequate for itinerant electrons, but in the present case we will justify the chosen model by the fact that the 3d band in Ho_2Co_{17} and Ho_2Fe_{17} is almost identical to the 3d band in the pure Co and Fe metals for which Liu (1976) have successfully used a localized quasi-spin picture to describe the ground state magnetic excitations. The crystal field anisotropy on the Co and Fe sites in Ho_2Co_{17} and Ho_2Fe_{17} is, however, much larger than in the pure transition metals, and the pseudo-spin description is unrealistic for the crystalline electric field in itinerant electron systems, but since the main influence of the 3d anisotropy on the excitation spectrum is to change the $\underline{q} = \underline{0}$ energy gap of the transition metal mode and to slightly modify the region where the two dispersive modes cross, we can use the concept of quasi-spins to introduce these changes. However, the actual value of the deduced anisotropy parameter should only be used as a qualitative measure of the transition metal sublattice anisotropy. Under the assumption that the rare earth and the optic transition metal modes are well separated in energy, the proposed linear spin-wave model can be solved analytically, and the interpretation will be limited by:

a) Only a linear combination of the axial crystal field parameters (B_2^0, B_4^0 and B_6^0) plus the basal plane crystal field parameter (B_6^6) can be deduced for the rare earth sites.

b) Only average transition metal - transition metal and rare earth - transition metal exchange constants can be deduced,

and these parameters should only be used in mean field calculations of the molecular fields on the rare earth and transition metal sites.

c) Only qualitative arguments can be given about the anisotropy of the 3d sublattice.

5.3. Experimental results

In the present experiments on Ho_2Co_{17} and Ho_2Fe_{17} we have observed two rather than four non degenerate rare earth modes, and since all ground state rare earth excitations will have energies in the investigated range of energy transfers, the dispersive rare earth mode must be a non degenerate in-phase mode of the four rare earth ions in the unit cell, and the non dispersive mode must be a tripply degenerate out-of-phase mode. Consequently the crystalline electric field of the two rare earth sites is identical. The single ion anisotropy of the rare earth sites is therefore determined by the charge distribution from the nearest neighbour transition metal ions (which are almost identical for the two rare earth sites) rather than by the influence from the more distant rare earth neighbours, which according to point charge calculations (Creedan and Rao 1973) would favour an easy basal plane for one of the sites, and an easy axis for the other.

Within the experimental accuracy no dispersion of the flat mode could be observed, and hence we can conclude that the rare earth - rare earth exchange is negligible.

5.3.1. Ho_2Co_{17}

For Ho_2Co_{17} the transition metal mode could only be observed for energy transfers less than the energy of the localized mode, i.e. it can only be seen when the 3d sublattice couples to the rare earth system. As soon as the precession of the 4f moments dies out, the transition metal mode is too weak to be observed. The same effect has been observed in $HoCo_2$ and $ErCo_2$ (Koon and Rhyne 1979), but the reason for this behaviour has not yet been found.

For Ho_2Co_{17} the transition metal mode is very steep, and the rare earth and the optic transition metal modes are well separated, as we have assumed in our model. From the deduced 3d-3d exchange constant, a mean field ordering temperature of 1257 ± 115 K was deduced. The observed ordering temperature is 1178 K, and we can conclude that the average molecular field on the transition metal sites is in agreement with experiments. The crystal field anisotropy of the Co sublattice was found to favour an easy basal plane.

From the molecular field on the rare earth sites, deduced from the rare earth - transition metal exchange and the deduced rare earth crystal field parameters B_2^0 and B_6^6 (B_4^0 and B_6^0 were assumed to be negligible) the magnetization curve and the temperature dependence of the localized mode - both intensity and energy transfers - could be predicted in agreement with experiments.

From the study of the macroscopic anisotropy parameters (Clausen and Nielsen (1981)), it could be concluded that the higher order axial anisotropy constants corresponding to B_4^0 and B_6^0 could be neglected. The predicted macroscopic anisotropy constants k_1 and k_4 were of correct sign, but both were an order of magnitude larger than the observed values. Despite this discrepancy, we can conclude that for Ho_2Co_{17} our simple model yields a consistent quantitative description of several independently observable magnetic properties for which the mean field approximation is valid for the 3d sublattice. It is of course beyond the scope of the model to describe magnetic interactions which are sensitive to the difference of the magnetic properties at the different 3d sites.

5.3.2. Ho_2Fe_{17}

For Ho_2Fe_{17} the energy separation of the optic Fe modes and the Ho modes is much smaller than in Ho_2Co_{17}, making the approximations of well separated modes from the two subsystems less justified.

For Ho_2Fe_{17} the Fe-Fe exchange interactions was found to be anisotropic, however the mean field ordering temperature of 300 ± 90 K derived from the 3d-3d exchange constant were in agreement with the observed ordering temperature of 335 K. Because of the two ion anisotropy of the Fe sublattice, no conclusive statements about the single ion anisotropy of the Fe sublattice can be given.

From the molecular field on the rare earth sites, deduced from the Ho-Fe exchange constant and the deduced crystal field parameters B_2^0 and B_6^6 for the rare earth sites (B_4^0 and B_6^0 were assumed to be negligible), the temperature dependence of the localized mode could be explained qualitatively, but the predicted temperature dependence of the intensity of the scattering showed some deviations from the observations. The macroscopic anisotropy measurements on Ho_2Fe_{17} showed that the higher order crystal field terms (B_4^0) could not be neglected, and the neglect of B_4^0 in the analysis of the localized mode is presumably the reason for the discrepancy between the observed and calculated scattering. The macroscopic anisotropy parameters calculated from the deduced crystal field parameters B_2^0 and B_6^6 were about an order of magnitude larger than observed.

For Ho_2Fe_{17} our simple model gives a consistent qualitative description of the performed experiments, but because the Fe ions are much more sensitive to changes in the local symmetry than the Co ions, a quantitative description of the magnetic interactions in Ho_2Fe_{17} will require a much more complicated model, taking two-ion anisotropy, higher order anisotropy constants and presumably magnetostriction into account.

ACKNOWLEDGEMENTS

The work described in this report was carried out at the Physics Department of Risø National Laboratory and the author is grateful for the excellent working conditions and never failing assistance provided by the scientists and technicians of the neutron scattering group.

I am indebted to my supervisors Professor V. Frank, Department of Electro Physics, The Technical University of Denmark, for his interest and assistance, and Bente Lebech, Risø National Laboratory, for her friendship, encouragement and cooperation. Thanks are also due to A. Nørlund Christensen, Department of Inorganic Chemistry, University of Aarhus, for growing the samples and performing X-ray analyses of the crystallographic properties.

Special thanks are due to P.-A. Lindgård for suggesting the problem and for many discussions. Hans Skriver, J.K. Kjems and J.J. Rhyne are also gratefully acknowledged for their encouragement and for many useful discussions.

Thanks are also due to Lone Astradsson, Kæth Kjøller, Gerda Stauning and Alice Thomsen both for typing and linguistic assistance throughout this study, and to Agnete Michelsen and Tora Skov for carefully drawing all the figures.

REFERENCES

ANIMALU, O.E. (1977). Intermediate Quantum Theory of Crystaline Solids (Prentice-Hall, Englewood Cliffs, N. J.) 516 pp.

BETHE, H. and SOMMERFELD, A. (1933). Handbuch der Physik 24, part 2 (Springer, Berlin) p. 595.

BETTERIDGE, W. (1979). Prog. in Materials Science 24, 51-142.

BOZORTH, R.M. (1951). Ferromagnetism (The Bell Telephone Laboratories Series) (Van Nostrand, New York) 985 pp.

BUSCHOW, K.H.J. (1971). Phys. Status Solidi A 7, 199-210.

CHRISTENSEN, A. NØRLUND and HAZELL, R.G. (1980). Acta Chem. Scand. A34, 455-459.

CLAUSEN, K. and NIELSEN, O.V. (1981). Magnetic Anisotropy in Single Crystals of Ho_2Co_{17} and Ho_2Fe_{17}. Submitted for publication (D.4).

DANIELSEN, O. and LINDGÅRD, P.-A. (1972). Quantum Mechanical Operator Equivalents Used in the Theory of Magnetism. Risø-Rep. 259, 93 pp.

DE GENNES, P.G. (1963). Magnetism 3. Edited by G.T. Rado and H. Suhl (Academic Press, New York) 115-147.

GIVORD, D. (1976). Thesis Grenoble A.O., 8856 CNRS.

GREEDAN, J.E. and RAO, V.U.S. (1973). J. Solid State Chem. 6, 387-395.

GUBBENS, P.C.M. (1977). Magnetic Properties of Rare Earth Ion Compounds (Delft University Press, Delft) 174 pp.

HOLSTEIN, T. and PRIMAKOFF, H. (1940). Phys. Rev. 58, 1098-1113.

HUTCHINGS,M.T. (1964). Solid State Phys. 16, 227-273.

KIRCHMAYR, H.R. and POLDY, C.A. (1978). J. Magn. Magn. Mater. 8, 1-42.

KITTEL, C. (1963). Quantum Theory of Solids (Wiley, New York) 435 pp.

KOON, N.C. and RHYNE, J.J. (1980). In: Proceedings of the International Conference on Crystaline Electric Field and Structural Effects in f-Electron Systems (Plenum Press, New York and London) 125-140.

LAFOREST, J., LEMAIRE, R., PAUTHENET, R. and SCHWEIZER, J. (1966). C. R. Acad. Sc. Ser. B. 262, 1260-1263.

LINDGÅRD, P.-A. and DANIELSEN, O. (1974). J. Phys. C. 7, 1523-1535.

LINDGÅRD, P.-A. and DANIELSEN, O. (1975). Phys. Rev. B. 11, 351-362.

LIU, S.H. (1976). Phys Rev. B 13, 3962-3971.

MALIK, S.K., ARLINGHAUS, F.J. and WALLACE, W.E. (1977). Phys. Rev. B. 16, 1242-1248.

MILLER, A.E., D'SILVA, T. and RODRIQUES, H. (1976). I.E.E.E. Trans. Magn. 12, 1006-1008.

RHYNE, J.J. and KOON, N.C. (1978). J. Appl. Phys. 49, 2133-2135.

RUDERMAN, M.A. and KITTEL, C. (1954). Phys. Rev. 96, 99-102.

SLATER, J.C. (1930). Phys. Rev. 35, 509-529.

STREEVER, R.L. (1979). Phys. Rev. B 19, 2704-2711.

SZPUNAR, B. and LINDGÅRD, P.-A. (1979). J. Phys. F 9, L55-L59.

TAYLOR, K.N.R. and POLDY, C.A. (1975). J. Phys. F 5, 1593-1606.

WALLACE, W.E. (1973). Rare Earth Intermetallics (Academic Press, New York and London) 266 pp.

WALLACE, W.E., SANKAR, S.G. and RAO, V.U.S. (1977). In: Structure and Bonding 33 (Springer, Berlin and Heidelberg), 1-55.

APPENDIX A

The Holstein-Primakoff transformation

In the Holstein-Primakoff transformations (Holstein and Primakoff, 1940), an analogy between the effects of the Bose operators on the harmonic oscillator wave functions, and the effect of the spin raising and lowering operators J^+ and J^- on the wave functions in the lowest J multiplet of a magnetic system is used to expand J^+, J^- and J^z in the Bose creation and annihilation operators.

In Fig. 19 we have sketched the level schemes for a harmonic oscillator and for two magnetic systems, both having the lowest J multiplet at much lower energies than the higher multiplets and having ground states which are fully magnetized either parallel to the z-axis or antiparallel to the z-axis. In the figure n denotes the n'th excited state. In the ferrimagnetic compounds to be examined in this thesis one of the sublattices will have $|J>$ as the ground state and the other $|-J>$.

Let's choose $|-J_R>$ as the ground state for the rare earth sublattice, then for $n < 2J$

$$J_R^+ \, |-J_R + n > = C \, |-J_R + (n+1) >$$

and

$$\sqrt{2J_R}\, a^\dagger \sqrt{1-a^\dagger a/2J_R}\, |\, n > = C \, |n+1 >$$

i.e.

$$J_R^+ \text{ and } \sqrt{2J_R}\, a^\dagger \sqrt{1-a^\dagger a/2J_R}$$

have the same matrix elements, and both excites the system from

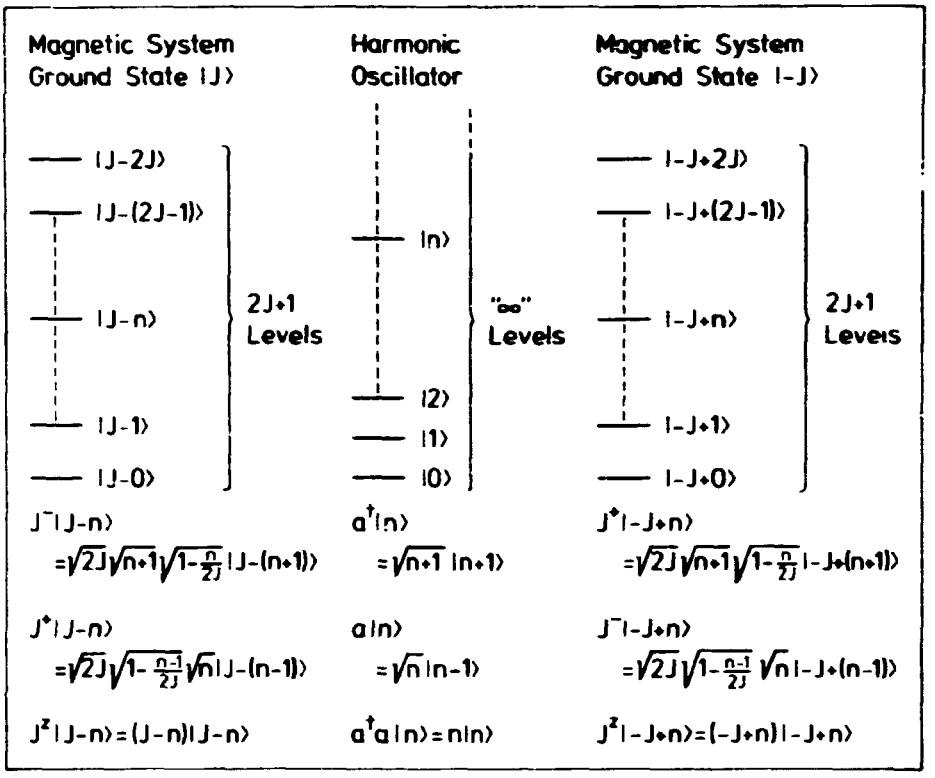

Fig. 19. Level schemes for a harmonic oscillator (centre) and for the lowest J multiplet of two magnetic systems, which are fully magnetized in the ground states either parallel (left) or anti-parallel (right) to the z-axis. At the bottom of the figure the effects of operating on the wave functions with the bose and spin operators are shown.

the n'th to the n+1'th excited state, similarly:

$$J_R^- \text{ corresponds to } \sqrt{2J_R}\ \sqrt{1-a^\dagger a/2J_R}\ a$$

and

$$J_R^z \text{ corresponds to } -J_R + a^\dagger a$$

The transition metal sites are magnetized antiparallel to the rare earth sites, and consequently the ground state of this system is $|J_T>$. For ease of notation the Bose operators are denoted b and $b^\dagger$ in the Holstein-Primakoff transformation of the trans-

ition metal sites. From Fig. 19 the following correspondence can be found:

J_T^+ corresponds to $\sqrt{2J_T}\ \sqrt{1-b^\dagger b/2J_T}\ b$

J_T^- corresponds to $\sqrt{2J_T}\ b^\dagger\ \sqrt{1-b^\dagger b/2J_T}$

and

J_T^z corresponds to $J_T - b^\dagger b$

From quantum mechanics it is found that

$$[J^+,J^-] = 2J^z \text{ and } [a,a^\dagger] = 1$$

are non-zero commutators among the spin operators and the Bose operators, respectively. Using the Holstein-Primakoff transformation,

$$[J_R^+,J_R^-] \text{ transforms into } 2J_R\left[a^\dagger\sqrt{1-\frac{a^\dagger a}{2J_R}},\ \sqrt{1-\frac{a^\dagger a}{2J_R}}\,a\right]$$

$$= 2J_R\left(a^\dagger(1-\frac{a^\dagger a}{2J_R})a - \sqrt{1-\frac{a^\dagger a}{2J_R}}\,aa^\dagger\,\sqrt{1-\frac{a^\dagger a}{2J_R}}\right)$$

$$= 2J_R\left(a^\dagger a - \frac{a^\dagger a^\dagger aa}{2J_R} - \sqrt{1-\frac{a^\dagger a}{2J_R}}\,(a^\dagger a+1)\,\sqrt{1-\frac{a^\dagger a}{2J_R}}\right)$$

$$= 2J_R\left(a^\dagger a - \frac{a^\dagger a^\dagger aa}{2J_R} - (1-\frac{a^\dagger a}{2J_R}) - \sqrt{1-\frac{a^\dagger a}{2J_R}}\,\sqrt{1-\frac{a^\dagger a}{2J_R}}\,a^\dagger a + 0\right)$$

$$= 2J_R\left(a^\dagger a - \frac{a^\dagger a^\dagger aa}{2J_R} - 1 + \frac{a^\dagger a}{2J_R} - a^\dagger a + \frac{a^\dagger aa^\dagger a}{2J_R}\right)$$

$$= 2J_R\left(-1 + \frac{a^\dagger a}{2J_R} - \frac{a^\dagger a^\dagger aa}{2J_R} + \frac{a^\dagger(a^\dagger a+1)a}{2J_R}\right)$$

$= 2(-J_R + a^\dagger a)$ corresponding to $2J_R^z$

and generally it can be shown that the Holstein-Primakoff transformation preserves the commutator relations, and consequently, when the lowest J multiplet provides a satisfactory description of the magnetic properties in which we are interested, and when temperatures or excitation energies are sufficiently low to avoid population of the non physical states with n greater than 2J+1, then the Holstein-Primakoff transformation can be used, and all calculations can be performed using the well known Bose operators and the harmonic oscillator wave functions.

APPENDIX B

Transformation of the Hamiltonian into a second order Hamiltonian in spin wave variables

This appendix gives a detailed description of the transformation from the spin operator Hamiltonian via the Holstein-Primakoff transformation and a subsequent Fourier transformation into a Hamiltonian of second order in the spin wave variables. The notation is defined in Section 2.1.

The Holstein-Primakoff transformation (Appendix A) for the rare earth sublattice is:

$$J_R^{i+}(\underline{\ell}) = \sqrt{2J_R}\, a_i^\dagger(\underline{\ell}) \sqrt{1 - \frac{a_i^\dagger(\underline{\ell}) a_i(\underline{\ell})}{2J_R}}$$

$$J_R^{i-}(\underline{\ell}) = \sqrt{2J_R} \sqrt{1 - \frac{a_i^\dagger(\underline{\ell}) a_i(\underline{\ell})}{2J_R}}\, a_i(\underline{\ell}) \qquad \text{(B.1)}$$

$$J_R^{iz}(\underline{\ell}) = -J_R + a_i^\dagger(\underline{\ell})\, a_i(\underline{\ell})$$

and for the transition metal sublattice:

$$J_T^{j+}(\underline{m}) = \sqrt{2J_T}\ \sqrt{1 - \frac{b_j^\dagger(\underline{m}) b_j(\underline{m})}{2J_T}}\ b_j(\underline{m})$$

$$J_T^{j-}(\underline{m}) = \sqrt{2J_T}\ b_j^\dagger(\underline{m})\ \sqrt{1 - \frac{b_j^\dagger(\underline{m}) b_j(\underline{m})}{2J_T}} \qquad \text{(B.2)}$$

$$J_T^{jz}(\underline{m}) = J_T - b_j^\dagger(\underline{m}) b_j(\underline{m})$$

In a neutron scattering experiment, the observed quantities are directly related to the Fourier transform of the Bose operators, and thus we introduce the spin wave variables $a_{\underline{q}}^{i\dagger}$, $a_{\underline{q}}^{i}$, $b_{\underline{q}}^{j\dagger}$ and $b_{\underline{q}}^{j}$ through the following equations:

$$a_i^\dagger(\underline{\ell}) = \frac{1}{\sqrt{N}} \sum_{\underline{q}} \exp\left(-i\underline{q}\cdot\underline{r}_R^i(\underline{\ell})\right) a_{\underline{q}}^{i\dagger}$$

$$a_i(\underline{\ell}) = \frac{1}{\sqrt{N}} \sum_{\underline{q}} \exp\left(i\underline{q}\cdot\underline{r}_R^i(\underline{\ell})\right) a_{\underline{q}}^{i} \qquad \text{(B.3)}$$

$$b_j^\dagger(\underline{m}) = \frac{1}{\sqrt{N}} \sum_{\underline{q}} \exp\left(i\underline{q}\cdot\underline{r}_T^j(\underline{m})\right) b_{\underline{q}}^{j\dagger}$$

$$b_j(\underline{m}) = \frac{1}{\sqrt{N}} \sum_{\underline{q}} \exp\left(-i\underline{q}\cdot\underline{r}_T^j(\underline{m})\right) b_{\underline{q}}^{j}$$

where N is the number of unit cells in the system.

The Hamiltonian consists of a two ion exchange term H_{ex} and a single ion crystal field term H_{CF}. In the two ion exchange term

$$H_{ex} = -\sum_{ij} J_{ij}\, \hat{J}_i \cdot \hat{J}_j$$

$\hat{J}_i$ and $\hat{J}_j$ always commutes ($J_{ii} = 0$) and a second order expansion of the Holstein-Primakoff transformation is sufficient. The single ion crystal field term H_{CF} can be expanded in $(J_i^z J_i^z)^n$ and $((J_i^+)^{2n} + (J_i^-)^{2n})$ and the full Holstein-Primakoff transform must be used in order to get a spin-wave Hamiltonian which is correct to second order in the magnon variables.

B.1. Transformation of H_{ex}

The exchange Hamiltonian for the R_nT_m compounds can be separated in three terms:

$$H_{ex} = H_{ex}^{TT} + H_{ex}^{RR} + H_{ex}^{RT}$$

Using Eq.(B.3), the second-order expansion of Eq.(B.1) can be written as:

$$J_R^{i+}(\underline{\ell}) = \sqrt{\frac{2J_R}{N}} \sum_{\underline{q}} \exp\left(-i\underline{q}\cdot\underline{r}_R^i(\underline{\ell})\right) a_{\underline{q}}^{i\dagger}$$

$$J_R^{i-}(\underline{\ell}) = \sqrt{\frac{2J_R}{N}} \sum_{\underline{q}} \exp\left(i\underline{q}\cdot\underline{r}_R^i(\underline{\ell})\right) a_{\underline{q}}^{i} \qquad \text{(B.4)}$$

$$J_R^{iz}(\underline{\ell}) = -J_R + \frac{1}{N} \sum_{\underline{q}} \sum_{\underline{q}'} \exp\left(-i(\underline{q}-\underline{q}')\cdot\underline{r}_R^i(\underline{\ell})\right) a_{\underline{q}}^{i\dagger} a_{\underline{q}'}^{i}$$

and similarly (B.2) can be expanded as:

$$J_T^{j+}(\underline{m}) = \sqrt{\frac{2J_T}{N}} \sum_{\underline{q}} \exp\left(-i\underline{q}\cdot\underline{r}_T^j(\underline{m})\right) b_{\underline{q}}^{j}$$

$$J_T^{j-}(\underline{m}) = \sqrt{\frac{2J_T}{N}} \sum_{\underline{q}} \exp\left(i\underline{q}\cdot\underline{r}_T^j(\underline{m})\right) b_{\underline{q}}^{j\dagger} \qquad \text{(B.5)}$$

$$J_T^{jz}(\underline{m}) = J_T - \frac{1}{N} \sum_{\underline{q}} \sum_{\underline{q}'} \exp\left(i(\underline{q}-\underline{q}')\cdot\underline{r}_T^j(\underline{m})\right) b_{\underline{q}}^{j\dagger} b_{\underline{q}'}^{j}$$

The 3d-3d part of the exchange Hamiltonian H_{ex}^{TT} is given by:

$$H_{ex}^{TT} = -\sum_{ij} \sum_{\underline{\ell}\underline{m}} J_{TT}^{ij}(\underline{\ell},\underline{m}) \left\{J_T^{i+}(\underline{\ell}) J_T^{j-}(\underline{m}) + J_T^{iz}(\underline{\ell}) J_T^{jz}(\underline{m})\right\}$$

$$= H^{+-} + H^{zz}$$

where

$$H^{+-} = -\frac{2J_T}{N} \sum_{ij} \sum_{\underline{\ell}\underline{m}} \sum_{\underline{q}\underline{q}'} J_{TT}^{ij}(\underline{\ell},\underline{m})\, b_{\underline{q}}^{i} b_{\underline{q}'}^{j\dagger} \exp\left(i\underline{q}'\cdot\underline{r}_T^j(\underline{m}) - i\underline{q}\cdot\underline{r}_T^i(\underline{\ell})\right)$$

$$= -\frac{2J_T}{N} \sum_{\underline{q}\underline{q}'} \sum_{ij} b_{\underline{q}}^{i}\, b_{\underline{q}'}^{j\dagger} \exp\left(i\underline{q}'\cdot\underline{d}_T^j - i\underline{q}\cdot\underline{d}_T^i\right) \sum_{\underline{\ell}\underline{m}} J_{TT}^{ij}(\underline{\ell},\underline{m}) \exp\left(i\underline{q}'\underline{m} - i\underline{q}\underline{\ell}\right)$$

The exchange constant $J_{TT}^{ij}(\underline{\ell},\underline{m})$ depends only on the lattice vector $\underline{L} = \underline{\ell}-\underline{m}$ and consequently:

$$\sum_{\underline{\ell}\underline{m}} J_{TT}^{ij}(\underline{\ell}-\underline{m}) \exp\left(i(\underline{q}'\cdot\underline{m} - \underline{q}\cdot\underline{\ell})\right) = \sum_{\underline{L}} J_{TT}^{ij}(\underline{L}) \exp\left(-i\underline{q}\cdot\underline{L}\right) \sum_{\underline{m}} \exp\left(i(\underline{q}'-\underline{q})\cdot\underline{m}\right)$$

$$= N\, \delta_{\underline{q}\underline{q}'} \sum_{\underline{L}} J_{TT}^{ij}(\underline{L}) \exp\left(-i\underline{q}\cdot\underline{L}\right)$$

i.e. H^{+-} can be written as

$$H^{+-} = -2J_T \cdot \sum_{ij} \sum_{\underline{q}} b_{\underline{q}}^{i}\, b_{\underline{q}}^{j\dagger}\, J_{TT}^{ij}(\underline{q})$$

with

$$J^{ij}_{TT}(\underline{q}) = \sum_{\underline{L}} J^{ij}_{TT}(\underline{L}) \exp\left(-i\underline{q}\cdot(\underline{L}+\underline{d}^i_T-\underline{d}^j_T)\right)$$

The second order expansion of H^{zz} can be found using

$$-J^{iz}_T(\underline{\ell})\ J^{jz}_T(\underline{m})$$

$$= \frac{J_T}{N} \sum_{\underline{q}\underline{q}'} \left(\exp\left(i(\underline{q}-\underline{q}')\cdot \underline{r}^j_T(\underline{m})\right) b^{j\dagger}_{\underline{q}}\, b^j_{\underline{q}'} + \exp\left(i(\underline{q}-\underline{q}')\cdot \underline{r}^i_T(\underline{\ell})\right) b^{i\dagger}_{\underline{q}}\, b^i_{\underline{q}'} \right) - J_T^2$$

and since $J^{ij}_{TT}(\underline{\ell},\underline{m})$ only depends on $\underline{L} = \underline{\ell} - \underline{m}$

$$\sum_{\underline{\ell}\underline{m}} J^{ij}_{TT}(\underline{\ell},\underline{m}) \exp\left(i(\underline{q}-\underline{q}')\cdot \underline{r}^j_T(\underline{m})\right)$$

$$= \sum_{\underline{L}} J^{ij}_{TT}(\underline{L}) \exp\left(i(\underline{q}-\underline{q}')\cdot(\underline{d}^j_T-\underline{L})\right) \sum_{\underline{\ell}} \exp\left(i(\underline{q}-\underline{q}')\cdot\underline{\ell}\right)$$

$$= N\, \delta_{\underline{q}\underline{q}'} \sum_{\underline{L}} J_{TT}(\underline{L})$$

H^{zz} can be written as:

$$H^{zz} = J_T \sum_{ij} \sum_{\underline{q}} J^{ij}_{TT}(\underline{0})\ (b^{i\dagger}_{\underline{q}} b^i_{\underline{q}} + b^{j\dagger}_{\underline{q}} b^j_{\underline{q}}) + H_o$$

where H_o is a constant, and can be neglected.

In a similar way H^{RR}_{ex} can be found as:

$$H^{RR}_{ex} = -J_R \sum_{\underline{q}} \sum_{ij} \left\{ 2\, J^{ij}_{RR}(\underline{q})\ a^{i\dagger}_{\underline{q}}\, a^j_{\underline{q}} - J^{ij}_{RR}(\underline{0})\,(a^{i\dagger}_{\underline{q}} a^i_{\underline{q}} + a^{j\dagger}_{\underline{q}} a^j_{\underline{q}}) \right\}$$

where

$$J^{ij}_{RR}(\underline{q}) = \sum_{\underline{L}} J^{ij}_{RR}(\underline{L}) \exp\left(-i\underline{q}\cdot(\underline{L} + \underline{d}^i_R - \underline{d}^j_R)\right)$$

The rare earth-transition metal exchange transforms as follows:

$$H^{RT}_{ex} = -\sum_{ij} \sum_{\underline{\ell}\underline{m}} J^{ij}_{RT}(\underline{\ell},\underline{m}) \left\{J^{i+}_R(\underline{\ell})J^{j-}_T(\underline{m}) + J^{i-}_R(\underline{\ell})J^{j+}_T(\underline{m}) + 2J^{iz}_R(\underline{\ell})J^{jz}_T(\underline{m})\right\}$$

The expansion of the first term is:

$$\sum_{\underline{\ell}\underline{m}} J^{ij}_{RT}(\underline{\ell},\underline{m})\ J^{i+}_R(\underline{\ell})\ J^{j-}_T(\underline{m})$$

$$= 2\sqrt{\frac{J_R\ J_T}{N}} \sum_{\underline{\ell}\underline{m}} \sum_{\underline{q}\underline{q}'} J^{ij}_{RT}(\underline{\ell},\underline{m})\ a^{i\dagger}_{\underline{q}} b^{j\dagger}_{\underline{q}'} \exp\left(-i\left[\underline{q}\cdot\underline{r}^i_R(\underline{\ell}) - \underline{q}'\cdot\underline{r}^j_T(\underline{m})\right]\right)$$

$$= 2\sqrt{\frac{J_R\ J_T}{N}} \sum_{\underline{q}\underline{q}'} a^{i\dagger}_{\underline{q}}\ b^{j\dagger}_{\underline{q}'} \exp\left(-i\left(\underline{q}\cdot\underline{d}^i_R - \underline{q}'\cdot\underline{d}^j_T\right)\right) \sum_{\underline{L}} J^{ij}_{RT}(\underline{L})\ \exp\left(-i\underline{q}'\cdot\underline{L}\right) \cdot \sum_{\underline{\ell}} \exp\left(-i(\underline{q}-\underline{q}')\cdot\underline{\ell}\right)$$

$$= 2\sqrt{J_R\ J_T} \sum_{\underline{q}} J^{ij}_{RT}(\underline{q})\ a^{i\dagger}_{\underline{q}}\ b^{j\dagger}_{\underline{q}}$$

with

$$J^{ij}_{RT}(\underline{q}) = \sum_{\underline{L}} J^{ij}_{RT}(\underline{L})\ \exp\left(-i\underline{q}\cdot(\underline{L} + \underline{d}^i_R - \underline{d}^j_T\right)$$

The second order expansion of the last term

$$2 \sum_{\underline{\ell}\underline{m}} J_{RT}^{ij}(\underline{\ell},\underline{m})\, J_R^{iz}(\underline{\ell})\, J_T^{jz}(\underline{m}) \quad \text{is:}$$

$$2 \sum_{\underline{q}\underline{q}'} \sum_{\underline{\ell}\underline{m}} J_{RT}^{ij}(\underline{\ell},\underline{m}) \left(\frac{J_R}{N} \exp\left(i(\underline{q}-\underline{q}') \cdot \underline{r}_T^j(\underline{m}) \right) b_{\underline{q}}^{j\dagger} b_{\underline{q}'}^{j} + \right.$$

$$\left. \frac{J_T}{N} \exp\left(-i(\underline{q}-\underline{q}') \cdot \underline{r}_R^i(\underline{\ell}) \right) a_{\underline{q}}^{i\dagger} a_{\underline{q}'}^{i} \right)$$

$$= 2 \sum_{ij} \sum_{\underline{q}} J_{RT}^{ij}(\underline{0}) \cdot \left(J_R\, b_{\underline{q}}^{j\dagger} b_{\underline{q}}^{j} + J_T\, a_{\underline{q}}^{i\dagger} a_{\underline{q}}^{i} \right)$$

i.e.

$$\mathcal{H}_{ex}^{RT} = -2 \sum_{\underline{q}} \sum_{ij} \left\{ \sqrt{J_R\, J_T} \left(J_{RT}^{ij}(\underline{q})\, a_{\underline{q}}^{i\dagger} b_{\underline{q}}^{j\dagger} + J_{RT}^{ij}(-\underline{q})\, a_{\underline{q}}^{i} b_{\underline{q}}^{j} \right) \right.$$

$$\left. + J_{RT}^{ij}(\underline{0}) \left(J_R\, b_{\underline{q}}^{j\dagger} b_{\underline{q}}^{j} + J_T\, a_{\underline{q}}^{i\dagger} a_{\underline{q}}^{i} \right) \right\}$$

B.2. Transformation of $\mathcal{H}_{CF}$

The Bose operator expansions of the Stevens operators have been tabulated by Danielsen and Lindgård (1972), and to second order the crystal field Hamiltonian of these rare earth-transition metal systems can be written as: (see Section B.4.)

$$\sum_{\underline{\ell}} \left[A_R^i\, a_i^\dagger(\underline{\ell})\, a_i(\underline{\ell}) + B_R^i \left(a_i^\dagger(\underline{\ell})\, a_i^\dagger(\underline{\ell}) + a_i(\underline{\ell})\, a_i(\underline{\ell}) \right) \right]$$

for the rare earth sites and

$$\sum_{\underline{m}} \sum_{j} \left[A_T^j \, b_j^\dagger(\underline{m}) \, b_j(\underline{m}) + B_T^j \left(b_j^\dagger(\underline{m}) \, b_j^\dagger(\underline{m}) + b_j(\underline{m}) \, b_j(\underline{m}) \right) \right]$$

for the transition metal sites.

These expressions can be transformed using:

$$\sum_{\underline{\ell}} a_i^\dagger(\underline{\ell}) \, a_i(\underline{\ell}) = \sum_{\underline{q}} a_{\underline{q}}^{i\dagger} a_{\underline{q}}^i$$

and

$$\sum_{\underline{\ell}} a_i^\dagger(\underline{\ell}) a_i^\dagger(\underline{\ell}) = \frac{1}{N} \sum_{\underline{q}\underline{q}'} a_{\underline{q}}^{i\dagger} a_{\underline{q}'}^{i\dagger} \exp\left(-i(\underline{q}+\underline{q}')\cdot \underline{d}_R^i\right) \sum_{\underline{\ell}} \exp\left(-i(\underline{q}+\underline{q}')\cdot\underline{\ell}\right)$$

$$= \sum_{\underline{q}} a_{\underline{q}}^{i\dagger} \, a_{-\underline{q}}^{i\dagger}$$

hence for the rare earth sublattice

$$H_{CF}(R) = \sum_i \sum_{\underline{q}} \left\{ A_R^i \, a_{\underline{q}}^{i\dagger} a_{\underline{q}}^i + B_R^i \left(a_{\underline{q}}^{i\dagger} a_{-\underline{q}}^{i\dagger} + a_{\underline{q}}^i a_{-\underline{q}}^i \right) \right\}$$

and for the transition metal sublattice

$$H_{CF}(T) = \sum_j \sum_{\underline{q}} \left\{ A_T^j \, b_{\underline{q}}^{j\dagger} b_{\underline{q}}^j + B_T^j \left(b_{\underline{q}}^{j\dagger} b_{-\underline{q}}^{j\dagger} + b_{\underline{q}}^j b_{-\underline{q}}^j \right) \right\}$$

B.3. The Hamiltonian to second order in the magnon variables

From the results of the previous three paragraphs the total Hamiltonian can be written as:

$$H = \sum_{\underline{q}} \Bigg[\sum_{ij} \Bigg\{ J_T \Big(J_{TT}^{ij}(\underline{0}) \, [b_{\underline{q}}^{i\dagger} b_{\underline{q}}^i + b_{\underline{q}}^{j\dagger} b_{\underline{q}}^j] - 2 \, J_{TT}^{ij}(\underline{q}) \, b_{\underline{q}}^i b_{\underline{q}}^{j\dagger} \Big)$$

$$+ J_R\Big(J^{ij}_{RR}(\underline{0})\ [a^{i\dagger}_{\underline{q}}a^{i}_{\underline{q}} + a^{j\dagger}_{\underline{q}}a^{j}_{\underline{q}}] - 2\ J^{ij}_{RR}(\underline{q})\ a^{i\dagger}_{\underline{q}}a^{j}_{\underline{q}}\Big)$$

$$- 2\ J^{ij}_{RT}(\underline{0})\ [J_R\ b^{j\dagger}_{\underline{q}}b^{j}_{\underline{q}} + J_T\ a^{i\dagger}_{\underline{q}}a^{i}_{\underline{q}}]$$

$$- 2\sqrt{J_R\ J_T}\ \Big(J^{ij}_{RT}(\underline{q})\ a^{i\dagger}_{\underline{q}}b^{j\dagger}_{\underline{q}} + J^{ij}_{RT}(-\underline{q})\ a^{i}_{\underline{q}}b^{j}_{\underline{q}}\Big)\ \Big\}$$

$$+ \sum_i \Big\{\ A^i_R\ a^{i\dagger}_{\underline{q}}a^{i}_{\underline{q}} + B^i_R(a^{i\dagger}_{\underline{q}}a^{i\dagger}_{-\underline{q}} + a^{i}_{\underline{q}}a^{i}_{-\underline{q}})\ \Big\}$$

$$+ \sum_j \Big\{\ A^j_T\ b^{j\dagger}_{\underline{q}}b^{j}_{\underline{q}} + B^j_T(b^{j\dagger}_{\underline{q}}b^{j\dagger}_{-\underline{q}} + b^{j}_{\underline{q}}b^{j}_{-\underline{q}})\ \Big\}\ \Big] + H'$$

where H' is a $\underline{q}$ independent constant,

$$J^{ij}_{\alpha\beta}(\underline{q}) = \sum_{\underline{L}} J^{ij}_{\alpha\beta}(\underline{L})\exp\Big(-i\underline{q}(\underline{L}+\underline{d}^i_\alpha-\underline{d}^j_\beta)\Big)$$

and $\underline{L}$ is a lattice vector.

B.4. Relations between A_α, B_α and the crystal field parameters B^m_ℓ

The crystal field Hamiltonian, which in the c-axis representation can be written as:

$$H^c_{CF} = B^0_2O^0_2 + B^0_4O^0_4 + B^0_6O^0_6 + B^6_6O^6_6$$

is transformed to (Danielsen and Lindgård 1972)

$$H^b_{CF} = B^0_2(-\tfrac{1}{2}O^0_2 - \tfrac{3}{2}O^2_2)$$

$$+ B_4^0\left(\frac{3}{8}O_4^0 + \frac{5}{2}O_4^2 + \frac{35}{8}O_4^4\right)$$

$$+ B_6^0\left(-\frac{5}{16}O_6^0 - \frac{105}{32}O_6^2 - \frac{63}{16}O_6^4 - \frac{231}{32}O_6^6\right)$$

$$- B_6^6\left(\frac{1}{16}O_6^0 - \frac{15}{32}O_6^2 + \frac{3}{16}O_6^4 - \frac{1}{32}O_6^6\right)$$

when the quantization axis is along the b-axis instead of the c-axis (see Fig. 20).

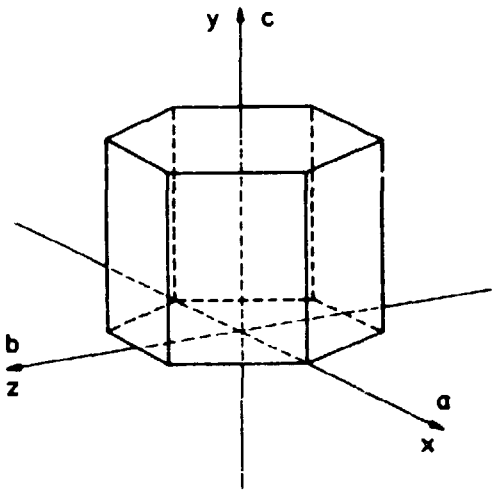

Fig. 20. The notation used for the different axes in a real space cell of the ferrimagnetic R_nT_m compounds with an easy b-axis.

To second order the Bose operator expansion of H_{CF}^b is given by (Lindgård and Danielsen 1974)

$$H_{CF}^b = \left(\frac{3\,S_2}{S_1}B_2^0 - \frac{30\,S_4}{S_1}B_4^0 + \frac{105\,S_6}{S_1}B_6^0 + \frac{21\,S_6}{S_1}B_6^6\right)a^\dagger a$$

$$+ \left(-\frac{3}{2}\sqrt{S_2}B_2^0 + \frac{15\,S_4}{\sqrt{S_2}}B_4^0 - \frac{315\,S_6}{2\sqrt{S_2}}B_6^0 + \frac{15\,S_6}{2\sqrt{S_2}}B_6^6\right)(a^\dagger a^\dagger + aa)$$

where

$$S_n = J\left(J - \tfrac{1}{2}\right)\ldots\ldots\ldots\left(J - \frac{n-1}{2}\right)$$

Table 10. The total angular momentum J and $S_n = J(J-\frac{1}{2})\ldots\ldots(J-\frac{n-1}{2})$ for Ho, Fe, and Co. (The g-factors of Fe and Co are assumed to be 2.00).

	J	S_1	S_2	S_4	S_6
Ho	8	8	60	2730	90090
Fe	1.05	1.05	1.58		
Co	0.80	0.80	0.24		

from Table 10 it can be seen that for Ho

$$H^{b}_{CF}(Ho) = (22.5\ B^{o}_{2} - 10238B^{o}_{4} + 1182431B^{o}_{6} + 236486B^{6}_{6})a^{\dagger}a$$

$$+ (-\ 11.62B^{o}_{2} + 5287B^{o}_{4} - 610605B^{o}_{6} + 87229B^{6}_{6})(a^{\dagger}a^{\dagger} + aa)$$

$$= A_{Ho}\ a^{\dagger}a + B_{Ho}(a^{\dagger}a^{\dagger} + aa)$$

i.e.

$$\begin{cases} B^{o}_{2} - 455.0\ B^{o}_{4} + 52552\ B^{o}_{6} = 0.0185\ A_{Ho} - 0.0502\ B_{Hc} \\ B^{6}_{6} = +2.467 \cdot 10^{-6} A_{Ho} + 4.777 \cdot 10^{-6} B_{Hc} \end{cases}$$

For the crystal field of Fe and Co the only parameter is B_2 (see Eq. (5))

$$H^{b}_{CF}(Fe) = 1.66\ B_{2}(Fe)\ b^{\dagger}b - 1.14\ B_{2}(Fe)\ (b^{\dagger}b^{\dagger} + bb)$$

$$= A_{Fe}\ b^{\dagger}b + B_{Fe}(b^{\dagger}b^{\dagger} + bb)$$

and

$$H^{b}_{CF}(Co) = 0.90\ B_2(Co)\ b^{\dagger}b - 0.73\ B_2(Co)\ (b^{\dagger}b^{\dagger} + bb)$$

$$= A_{Co}\ b^{\dagger}b + B_{Co}(b^{\dagger}b^{\dagger} + bb)$$

i.e.

$$B_2(Fe) = 0.602\ A_{Fe} \text{ and } B_{Fe}/A_{Fe} = -0.691$$

$$B_2(Co) = 1.11\ A_{Co} \text{ and } B_{Co}/A_{Co} = -0.816 \qquad (B.6)$$

B.5. Commutator relations between magnon operators

The commutator relations between Bose operators can be written as:

$$\left[a_i(\underline{\ell}),\ a^{\dagger}_j(\underline{m})\right] = \delta_{ij}\ \delta_{\underline{\ell}\underline{m}}$$

and similarly for b and $b^{\dagger}$. The commutator relations for the magnon variables

$$\left[a^{i}_{\underline{q}},\ a^{j\dagger}_{\underline{q}'}\right]$$

can be evaluated using

$$a^{j\dagger}_{\underline{q}'} = \frac{1}{\sqrt{N}} \sum_{\underline{m}} \exp\left(i\underline{q}'\cdot\underline{r}^{j}_{R}(\underline{m})\right)\ a^{\dagger}_j(\underline{m})$$

and

$$a^{i}_{\underline{q}} = \frac{1}{\sqrt{N}} \sum_{\underline{\ell}} \exp\left(-i\underline{q}\cdot\underline{r}^{i}_{R}(\underline{\ell})\right)\ a_i(\underline{\ell})$$

i.e

$$\left[a_{\underline{q}}^{i},\ a_{\underline{q}'}^{j\dagger}\right] = \frac{1}{N}\sum_{\underline{\ell}\underline{m}} \exp\left(i\left(\underline{q}'\cdot\underline{r}_R^j(\underline{m}) - \underline{q}\cdot\underline{r}_R^i(\underline{\ell})\right)\right)\left[a_i(\underline{\ell}), a_j^{\dagger}(\underline{m})\right]$$

$$= \frac{\delta_{ij}}{N}\ \exp\left(i\left(\underline{q}'-\underline{q}\right)\cdot\underline{d}_R^i\right)\sum_{\underline{\ell}\underline{m}}\ \delta_{\underline{\ell}\underline{m}}\exp\left(i\left(\underline{q}'-\underline{q}\right)\cdot\underline{\ell}\right)$$

$$= \delta_{ij}\ \delta_{\underline{q}'\underline{q}}$$

and the only non zero commutator relations between spin-wave variables can be written as:

$$\left[a_{\underline{q}}^{i},\ a_{\underline{q}}^{i\dagger}\right] = 1$$

and

$$\left[b_{\underline{q}}^{j},\ b_{\underline{q}}^{j\dagger}\right] = 1$$

APPENDIX C

The spin-wave solution

C.1. The equations of motion for the spin-wave variables

The time dependence of the magnon variables is given by the factor $\exp(-i\omega t)$, and the equation of motion by

$$i\hbar\ \frac{d\ a_{\underline{q}}^{n}(t)}{dt} = \left[a_{\underline{q}}^{n}(t),\ H\right]$$

i.e.

$$\dot{a}_{\underline{q}}^{n} = \left[a_{\underline{q}}^{n},\ H\right] \tag{C.1}$$

where H is the Hamiltonian given in Section 3.3 and

$$a_{\underline{q}}^{n}(t) = a_{\underline{q}}^{n} \exp(-i\omega t)$$

The solution to Eq. (C.1) can be written as:

$$\dot{a}_{\underline{q}}^{n} = a_{\underline{q}}^{n}\left[\sum_{j} J_R J_{RR}^{nj}(\underline{0}) + \sum_{i} J_R J_{RR}^{in}(\underline{0}) - 2J_T \sum_{j} J_{RT}^{nj}(\underline{0}) + A_R^n\right]$$

$$+ \sum_{j} a_{\underline{q}}^{j}\left[-2J_R J_{RR}^{nj}(\underline{q})\right]$$

$$+ \sum_{j} b_{\underline{q}}^{j\dagger}\left[-2\sqrt{J_R J_T}\, J_{RT}^{nj}(\underline{q})\right]$$

$$+ a_{-\underline{q}}^{n\dagger} B_R^n \tag{C.1.a}$$

and equivalently:

$$\dot{a}_{-\underline{q}}^{n\dagger} = -a_{-\underline{q}}^{n\dagger}\left[J_R \sum_{j} J_{RR}^{nj}(\underline{0}) + J_R \sum_{i} J_{RR}^{in}(\underline{0}) - 2J_T \sum_{j} J_{RT}^{nj}(\underline{0}) + A_R^n\right]$$

$$- \sum_{i} a_{-\underline{q}}^{i\dagger}\left[-2J_R J_{RR}^{in}(-\underline{q})\right]$$

$$- \sum_{j} b_{-\underline{q}}^{j}\left[-2\sqrt{J_R J_T}\, J_{RT}^{nj}(\underline{q})\right]$$

$$- a_{\underline{q}}^{n} B_R^n \tag{C.1.b}$$

For the transition metal sites:

$$\hbar\omega\, b^{n}_{-\underline{q}} = b^{n}_{-\underline{q}} \left[J_T \sum_j J^{nj}_{TT}(\underline{0}) + J_T \sum_i J^{in}_{TT}(\underline{0}) - 2J_R \sum_i J^{in}_{RT}(\underline{0}) + A^{n}_{T} \right]$$

$$+ \sum_i b^{i}_{-\underline{q}} \left[-2J_T\, J^{in}_{TT}(-\underline{q}) \right]$$

$$+ \sum_i a^{i\dagger}_{-\underline{q}} \left[-2\sqrt{J_R J_T}\, J^{in}_{RT}(-\underline{q}) \right]$$

$$+ b^{n\dagger}_{\underline{q}}\, B^{n}_{T} \qquad \text{(C.1.c)}$$

and

$$\hbar\omega\, b^{n\,\dagger}_{\underline{q}} = - b^{n\dagger}_{\underline{q}} \left[J_T \sum_j J^{nj}_{TT}(\underline{0}) + J_T \sum_i J^{in}_{TT}(\underline{0}) - 2J_R \sum_i J^{in}_{RT}(\underline{0}) + A^{n}_{T} \right]$$

$$- \sum_j b^{j\dagger}_{\underline{q}} \left[-2J_T\, J^{nj}_{TT}(\underline{q}) \right]$$

$$- \sum_i a^{i}_{\underline{q}} \left[-2\sqrt{J_R J_T}\, J^{in}_{RT}(-\underline{q}) \right]$$

$$- b^{n}_{-\underline{q}}\, B^{n}_{T} \qquad \text{(C.1.d)}$$

If we assume that each site in the structure has inversion symmetry then

$$J^{ij}_{\alpha\beta}(\underline{q}) = J^{ij}_{\alpha\beta}(-\underline{q})$$

and the eigenvalue equations above Eqs. (C.1.a-d) can be written as:

$$\begin{Bmatrix} \underline{\underline{A}} & \underline{\underline{B}} \\ -\underline{\underline{B}} & -\underline{\underline{A}} \end{Bmatrix} \begin{Bmatrix} \underline{x}_{\underline{q}} \\ \underline{y}_{\underline{q}} \end{Bmatrix} = \hbar\omega \begin{Bmatrix} \underline{x}_{\underline{q}} \\ \underline{y}_{\underline{q}} \end{Bmatrix} \tag{C.2}$$

where

$$\underline{x}_{\underline{q}} = \begin{Bmatrix} a^{1}_{\underline{q}} \\ \vdots \\ a^{n}_{\underline{q}} \\ b^{1\dagger}_{\underline{q}} \\ \vdots \\ b^{m\dagger}_{\underline{q}} \end{Bmatrix} \text{ and } \underline{y}_{\underline{q}} = \begin{Bmatrix} a^{1\dagger}_{-\underline{q}} \\ \vdots \\ a^{n\dagger}_{-\underline{q}} \\ b^{1}_{-\underline{q}} \\ \vdots \\ b^{m}_{-\underline{q}} \end{Bmatrix} \tag{C.3}$$

The precession of a spin-wave mode is given by ω and a wave vector $\underline{q}$ via the two terms $\exp(i(\underline{q}\cdot\underline{r}-\omega t))$ and $\exp(-i(\underline{q}\cdot\underline{r}-\omega t)) = \exp(i(-\underline{q}\cdot\underline{r}-(-\omega)t))$ i.e. a magnon mode can be calculated by solving (C.1) for both

$$h|\omega|; \begin{Bmatrix} \underline{x}_{\underline{q}} \\ \underline{y}_{\underline{q}} \end{Bmatrix}$$

and

$$-h|\omega|; \begin{Bmatrix} \underline{x}_{-\underline{q}} \\ \underline{y}_{-\underline{q}} \end{Bmatrix}$$

but the two solutions are inter related because in the two cases Eq.(C.1) can be written as

$$(\underline{\underline{A}} - M|\omega|\underline{\underline{E}})\ \underline{x}_{\underline{q}} + \underline{\underline{B}}\ \underline{y}_{\underline{q}} = 0$$

$$\underline{\underline{B}}\ \underline{x}_{\underline{q}} + (\underline{\underline{A}} + M|\omega|\underline{\underline{E}})\ \underline{y}_{\underline{q}} = 0$$

and

$$(\underline{\underline{A}} + M|\omega|\underline{\underline{E}})\ \underline{x}_{-\underline{q}} + \underline{\underline{B}}\ \underline{y}_{-\underline{q}} = 0$$

$$\underline{\underline{B}}\ \underline{x}_{-\underline{q}} + (\underline{\underline{A}} - M|\omega|\underline{\underline{E}})\ \underline{y}_{-\underline{q}} = 0$$

where $\underline{\underline{E}}$ is the unit matrix.

i.e.

$$\begin{aligned} \underline{x}_{\underline{q}} &= \underline{y}_{-\underline{q}} \\ \underline{y}_{\underline{q}} &= \underline{x}_{-\underline{q}} \end{aligned} \tag{C.4}$$

(strictly speaking $\underline{x}_{\underline{q}} = K \cdot \underline{y}_{-\underline{q}}$ and $\underline{y}_{\underline{q}} = K \cdot \underline{x}_{-\underline{q}}$ where K is a constant) using Eq.(C.2), Eq.(C.4) can be written as

$$\begin{aligned} a^{i\dagger}_{\underline{q}} &= a^{i}_{\underline{q}} \\ b^{j\dagger}_{\underline{q}} &= b^{j}_{\underline{q}} \end{aligned} \tag{C.5}$$

and Eq.(B.5, p. 66) takes the following form:

$$J^{j+}_{T}(\underline{m},t) = \sqrt{\frac{2J_T}{N}} \sum_{\underline{q}} [b^{j}_{-\underline{q}} \exp(i(\underline{q}\cdot\underline{r}^{j}_{T}(\underline{m})-\omega t)) + b^{j}_{\underline{q}} \exp(-i(\underline{q}\cdot\underline{r}^{j}_{T}(\underline{m})-\omega t))]$$

$$J^{j-}_{T}(\underline{m},t) = \sqrt{\frac{2J_T}{N}} \sum_{\underline{q}} [b^{j\dagger}_{\underline{q}} \exp(i(\underline{q}\cdot\underline{r}^{j}_{T}(\underline{m})-\omega t)) + b^{j\dagger}_{-\underline{q}} \exp(-i(\underline{q}\cdot\underline{r}^{j}_{T}(\underline{m})-\omega t))]$$

i.e.

$$J_T^{j\,a}(\underline{m},t) = \sqrt{\frac{2J_T}{N}}\,(b^j_{-\underline{q}} + b^{j\dagger}_{\underline{q}})\,\cos(\underline{q}\cdot\underline{r}^j_T(\underline{m})-\omega t)$$

$$J_T^{j\,c}(\underline{m},t) = \sqrt{\frac{2J_T}{N}}\,(b^j_{-\underline{q}} - b^{j\dagger}_{\underline{q}})\,\sin(\underline{q}\cdot\underline{r}^j_T(\underline{m})-\omega t)$$

where the a and c directions are given in Fig. 20 and we have used the identities

$$J^+ = J^a + i\,J^c \text{ and } J^- = J^a - i\,J^c$$

In a similar way Eq.(B.4, p. 63) can be rewritten as

$$J_R^{i\,a}(\underline{\ell},t) = \sqrt{\frac{2J_R}{N}}\,(a^{i\dagger}_{-\underline{q}} + a^i_{\underline{q}})\,\cos(\underline{q}\cdot\underline{r}^i_R(\underline{\ell})-\omega t)$$

$$J_R^{i\,c}(\underline{\ell},t) = \sqrt{\frac{2J_R}{N}}\,(a^{i\dagger}_{-\underline{q}} - a^i_{\underline{q}})\,\sin(\underline{q}\cdot\underline{r}^i_R(\underline{\ell})-\omega t)$$

C.2. Spin-wave dispersion

The magnon energies $\hbar|\omega|$ for the low lying modes can be calculated from Eq.(C.1) using the approximations described in Section 3.5:

$$b^i_{\underline{q}},\ b^{i\dagger}_{\underline{q}},\ A^i_R,\ B^i_R,\ \sum_j J^{ij}_{RT}(\underline{q}) \text{ all independent af i}$$

and $J_{RR} = 0$.

Eqs.(C.1.a-d) can now be written as:

$$\hbar\omega\ a^n_{\underline{q}} = \left(-\frac{2J_T}{N_R}\,J_{RT}(\underline{0}) + A_R\right)\,a^n_{\underline{q}}$$

$$- 2 \frac{\sqrt{J_R J_T}}{N_R} J_{RT}(\underline{q})\ b^{\dagger}_{\underline{q}}$$

$$+ B_R\ a^{n\dagger}_{-\underline{q}} \qquad \text{(C.6.a)}$$

$$\hbar\omega\ a^{n\dagger}_{-\underline{q}} = -\left(-\frac{2J_T}{N_R} J_{RT}(\underline{0}) + A_R\right) a^{n\dagger}_{-\underline{q}}$$

$$+ 2 \frac{\sqrt{J_R J_T}}{N_R} J_{RT}(\underline{q})\ b_{-\underline{q}}$$

$$- B_R\ a^{n}_{\underline{q}} \qquad \text{(C.6.b)}$$

and

$$\hbar\omega\ b_{-\underline{q}} = \left(\frac{2J_T}{N_T}\left(J_{TT}(\underline{0}) - J_{TT}(\underline{q})\right) - \frac{2J_R}{N_T} J_{RT}(\underline{0}) + A_T\right) b_{-\underline{q}}$$

$$- 2 \frac{\sqrt{J_R J_T}}{N_R N_T} J_{RT}(-\underline{q}) \sum_i a^{i\dagger}_{-\underline{q}}$$

$$+ B_T\ b^{\dagger}_{\underline{q}} \qquad \text{(C.6.c)}$$

and

$$\hbar\omega\ b^{\dagger}_{\underline{q}} = -\left(\frac{2J_T}{N_T}\left(J_{TT}(\underline{0}) - J_{TT}(\underline{q})\right) - \frac{2J_R}{N_T} J_{RT}(\underline{0}) + A_T\right) b^{\dagger}_{\underline{q}}$$

$$+ 2 \frac{\sqrt{J_R J_T}}{N_R N_T} J_{RT}(-\underline{q}) \sum_i a^{i}_{\underline{q}}$$

$$- B_T\ b_{-\underline{q}} \qquad \text{(C.6.d)}$$

where $J_{\alpha\beta}(\underline{q}) = \sum_{ij} J^{ij}_{\alpha\beta}(\underline{q})$

For the R_2T_{17} compounds $J_{\alpha\beta}(\underline{q}) = J_{\alpha\beta}(-\underline{q})$ and the eigen-value equation can be written as (C.2)

where $\underline{x}_{\underline{q}} = \begin{Bmatrix} a^1_{\underline{q}} \\ a^2_{\underline{q}} \\ a^3_{\underline{q}} \\ a^4_{\underline{q}} \\ b^\dagger_{\underline{q}} \end{Bmatrix}$ and $\underline{y}_{\underline{q}} = \begin{Bmatrix} a^{1\dagger}_{-\underline{q}} \\ a^{2\dagger}_{-\underline{q}} \\ a^{3\dagger}_{-\underline{q}} \\ a^{4\dagger}_{-\underline{q}} \\ b_{-\underline{q}} \end{Bmatrix}$

$$\underline{\underline{A}} = \begin{Bmatrix} a & 0 & 0 & 0 & c(\underline{q}) \\ 0 & a & 0 & 0 & c(\underline{q}) \\ 0 & 0 & a & 0 & c(\underline{q}) \\ 0 & 0 & 0 & a & c(\underline{q}) \\ -c(\underline{q})/N_T & -c(\underline{q})/N_T & -c(\underline{q})/N_T & -c(\underline{q})/N_T & b(\underline{q}) \end{Bmatrix}$$

$$\underline{\underline{B}} = \begin{Bmatrix} d_R & 0 & 0 & 0 & 0 \\ 0 & d_R & 0 & 0 & 0 \\ 0 & 0 & d_R & 0 & 0 \\ 0 & 0 & 0 & d_R & 0 \\ 0 & 0 & 0 & 0 & d_T \end{Bmatrix}$$

where

$$a = A_R - \frac{2J_T}{N_R} J_{RT}(\underline{0})$$

$$b(\underline{q}) = \frac{2J_T}{N_T}\left(J_{TT}(\underline{q}) - J_{TT}(\underline{0})\right) + \frac{2J_R}{N_T} J_{RT}(\underline{0}) - A_T$$

$$c(\underline{q}) = -2\frac{\sqrt{J_R J_T}}{N_R} J_{RT}(\underline{q})$$

$$d_R = B_R$$

$$d_T = -B_T$$

N_R = the number of rare earth atoms in the unit cell

N_T = the number of transition metal atoms in the unit cell

J_R, J_T are the total angular momenta of the rare earth ions and the pseudo-spin of the transition metal ions.

Using simple matrix operations the eigen-value problem in Eq. (C.2) can be reduced to solving Eq. (C.7)

$$\det \begin{Bmatrix} \begin{pmatrix} a-\lambda & d_R \\ -d_R & -a-\lambda \end{pmatrix} & 0 & 0 & 0 & 0 & 0 & 0 & 0 \\ 0 & 0 & \begin{pmatrix} a-\lambda & d_R \\ -d_R & -a-\lambda \end{pmatrix} & 0 & 0 & 0 & 0 & 0 \\ 0 & 0 & 0 & 0 & \begin{pmatrix} a-\lambda & d_R \\ -d_R & -a-\lambda \end{pmatrix} & 0 & 0 & 0 \\ 0 & 0 & 0 & 0 & 0 & 0 & 0 & 0 \\ 0 & 0 & 0 & 0 & 0 & 0 & \begin{pmatrix} a-\lambda & 4c(\underline{q}) & d_R & 0 \\ -c(\underline{q})/N_T & b(\underline{q})-\lambda & 0 & d_T \\ d_R & 0 & a+\lambda & 4c(\underline{q}) \\ 0 & d_T & -c(\underline{q})/N_T & b(\underline{q})+\lambda \end{pmatrix} \end{Bmatrix} = 0 \quad (C.7)$$

For $\lambda = h\omega$

The solution to Eq.(C.7) is the triply degenerate $\underline{q}$ independent (nondispersive) solution:

$$(h\omega)^2 = a^2 - d_R^2$$

and the two $\underline{q}$ dependent (dispersive) solutions:

$$(h\omega)^2 = (a^2 - d_R^2 + b^2(\underline{q}) - d_T^2)/2 - c^2(\underline{q}) \cdot N_R/N_T$$

$$\pm \sqrt{(a^2-d_R^2-b^2(\underline{q})+d_T^2)^2/4 - N_R c^2(\underline{q})\,((a+b(\underline{q}))^2 - (d_R-d_T)^2)/N_T}$$

Sales distributors:
Jul. Gjellerup, Sølvgade 87,
DK-1307 Copenhagen K, Denmark

Available on exchange from:
Risø Library, Risø National Laboratory,
P. O. Box 49, DK-4000 Roskilde, Denmark

ISBN 87-550-0658-2
ISSN 0106-2840